Major elemental chemistry of geothermal springs from the Deccan traps: Solute sources and chemical fluxes

A thesis submitted in partial fulfillment of the requirements for the M.Sc. Degree Programme

By

Samarpan Mahato

20226406

Indian Institute of Science Education and Research

Pune 411008,India

March,2024

Under the guidance of

Dr. Gyana Ranjan Tripathy

Earth and Climate Science Department

IISER Pune

भारतीय विज्ञान शिक्षा एवं अनुसंधान संस्थान पुणे
INDIAN INSTITUTE OF SCIENCE EDUCATION AND RESEARCH PUNE
An Autonomous Institution of the Ministry of Education, Govt. of India

Certificate

This is to certify that this dissertation entitled ***Major elemental chemistry of Geothermal Springs from the Deccan traps: Solute sources and chemical fluxes*** submitted to IISER Pune in partial fulfillment of the requirements for the award of Degree of M.Sc. in Geology. This is a record of original research work carried out by Samarpan Mahato, during the period of study (2023 - 2024) in the Department of Earth and Climate Science under the guidance of Dr. Gyana Ranjan Tripathy, Associate Professor, Department of Earth and Climate Science.

Dr. Gyana Ranjan Tripathy
Associate Professor and Chair,
Department of Earth and Climate Science,
IISER PUNE, 411008

Dr. Gyana Ranjan Tripathy
(Supervisor)

Declaration

I hereby declare that this dissertation titled "**Major elemental chemistry of geothermal springs from the Deccan traps: Solute sources and chemical fluxes** " submitted for the M.Sc. degree program at the Indian Institute of Science Education and Research, Pune is my original work under the supervision of Dr. Gyana Ranjan Tripathy. All sources used in this dissertation have been duly acknowledged and cited by academic conventions and guidelines. Any assistance received during the research and writing process has been acknowledged appropriately. No part of this dissertation has been submitted for any other degree or qualification at any other institution.

Samarpan Mahato
M.Sc. Student,
Department of Earth and Climate Science,
IISER PUNE, 411008

Acknowledgment

I am thankful to several individuals who played any minor roles in the success of this dissertation. Firstly, I extend my sincere gratitude to my guide, Dr. Gyana Ranjan Tripathy for arranging the necessary funding for the field trip for this dissertation along with his support and guidance. I would also like to thank my expert Dr. Shreyas Managave for providing me with valuable insights in this thesis **.** This thesis could not have been successful without the constant support and guidance of my lab senior Mr. Rakesh Kumar Rout. I appreciate all the hard work and sincerity he put in towards teaching me and helping me with the analyses to finish this research project within time. I am also deeply indebted to Ms. Kruttika Mohapatra, Mr. Sanket Samal, and Ashis Tanay Behera for their immense help during the water sampling field. I also thank Ms. Subhashree Maity and Mr. Achyuth Venugopal for their help during this study. Lastly, I would like to thank my parents for their constant support.

List of Abbreviations

Hot springs- HS

Deccan Volcanic Province – DVP

Large Igneous Province – LIP

K-Pg- Cretaceous-Paleogene

West Coast Geothermal Province – WCGP

North North West- NNW

South South East - SSW

North West -NW

South East - SW

West Coast Fault- WCF

Normalized Inorganic Charge balance- NICB

List of Figures

List of Tables

Table of Contents

Abstract

Hot springs are largely originated through subsurface processes where surface water goes deep into the earth and get heated up by geothermal heat. These processes often occur in the areas of tectonic and volcanic activity. These spring waters, owing to their relatively higher temperature than surface water, have a higher solubility and hence, are characterized with higher solutes concentrations. This is an important solute source for the adjacent watersheds and are also capable of releasing substantial amounts of CO_2 to the atmosphere. Despite of its large significance, very few attempts are made to understand this process, particularly from Deccan traps, in India. In this study, major ion chemistry of the hot springs from the Deccan trap regions was investigated to ascertain solute source and also, to quantify the CO_2 release rate. In the Deccan region, hot springs are present along a linear belt along the west coast geothermal province, and they are supplying solute fluxes into the adjacent rivers of the western ghat. To achieve this goal, a field trip was carried out to the Deccan region for the collection of hot springs samples and river and groundwater during October 2023. All the geochemical analysis of the samples were carried at IISER Pune. The average dissolved silica and HCO_3 of the hot spring samples are 1047 ± 307 μM and 848 ± 1222 μM respectively. Most of the hot spring samples are indicating Na-Cl rich water which might indicate seawater mixing acting as a dominant solute supplier. Solute flux from the river is much higher than the hot spring mainly because of higher discharge of the river and the dilution effect. The average reservoir temperature for these geothermal springs is estimated to be 111 ± 14 °C by silica geothermometer and 128 ± 58 °C by Na/K geothermometer. The CO_2 release rate for the hot springs is computed by adopting a direct approach (Evans et al., 2008 and Tiwari et al., 2016) and found to be 4.6×10^5 moles/yr in total which is 3.8×10^4 times lower than that of the Himalayan hot springs. About half of the CO_2 consumption in the Deccan region is counter balanced through CO_2 release rate of the adjacent hot spring. Moreover, this study highlights the implications of Deccan hot springs in the context of solute supply and carbon cycle.

1. Chapter1

1.1 Introduction

Orogenesis refers to the process of the formation of mountains during the plate convergence in the destructive plate boundaries. This process in tectonically-active terrain accelerate the physical erosion rate, by facilitating continuous exposure of fresher rocks (silicates and carbonates). Intense silicate erosion in active young tropical mountain belts (e.g. Himalaya) is considered as one of the prime drivers of global Cenozoic cooling (Raymo and Ruddiman, 1992). These surface processes play a vital role in sequestering CO_2 from the atmosphere which helps in regulating the long-term carbon cycle. In contrast, there are other processes (e.g., geothermal springs) in these orogenic belts with high heat flow may release the CO_2 counterbalancing the consumption via silicate weathering (Irwin and Barnes, 1980). The effect of such CO_2 flux is less studied (Galy and France-Lanord, 1999; Quade et al., 2003; France-Lanord et al., 2003) and quantified globally. This flux can be quantified by using the dissolved inorganic carbon (DIC) of the geothermal springs. DIC can be produced from various sources and its $\delta^{13}C$ value reflects the source of the released CO_2 (Tiwari et al., 2014, 2016; Newell et al., 2008; Becker et al., 2008; Evans et al., 2008). It can come from (i) carbonate rock dissolution (ii) the metamorphic decarbonation (iii) CO_2 dissolved in meteoric water (iv) oxidation of organic matter in soil (soil / biogenic CO_2) and (v) mantle and magma degassing. The released CO_2 from different sources has unique $\delta^{13}C$ values (atmospheric CO_2, magma or mantle:< -3 to -8 ‰ metamorphic CO_2: -3 to +3 ‰, carbonates: around 0‰, organic source: < -22‰) (Dotsika et al., 2021; Wei et al.,2024). Efforts are made in the Himalayan region to quantify the metamorphic CO_2 degassing to the atmosphere by investigating the chemistry of geothermal springs (Tiwari et al., 2016; Newell et al., 2008; Becker et al., 2008; Evans et al., 2008). Evans et al., (2008) have quantified about 2×10^{11} mol a^{-1} of CO_2 via metamorphic decarbonation in the Himalayas, which accounts to 7 to 60 % of the flux released from volcanic arcs globally (Marty and Tolstikhin, 1998; Gorman and Kerrick, 2006). The estimated amount of CO_2 released into the atmosphere is 4 times higher than the CO_2 drawdown via the silicate weathering in these terrains. Extrapolation of the CO_2 efflux estimation for the whole Himalayan arc gives one-fourth of the global CO_2 consumption via silicate weathering (Gaillardet and Galy, 2008). A similar evidence was drawn by Becker et al., (2008) based on $\delta^{13}C$ isotope and thermodynamic modelling of chemical species dissolved in geothermal spring

water. Tiwari et al., (2016) quantified the CO_2 flux for the entire northwest Himalaya at about 2×10^{12} mol a^{-1} by combining their estimation with earlier study. Perrier et al., 2008 found radon-222 concentration in the geothermal water of Nepal Himalayan region varies from 0.25 to 3 Ba L^{-1} and found a correlation between the radon and the CO_2 flux.

Hot springs, in addition to its role in the CO_2 cycle, also serve as geothermal energy worldwide and are treated as renewable resources of energy (Chandrasekhar et al., 2016). Several trace elements (B, Ba, Sr, As, and P, etc.) are also being supplied by hot springs to the global ocean (Evans et al., 2001, 2004; Hren et al., 2007; Lü et al., 2014; Fringes and Buss, 2019). Furthermore, hot springs supply substantial alkalinity to the ocean which controls the ocean pH. Hot springs are found to be the dominant source of radiogenic Sr in the Himalayan river catchments, which may affect the global oceanic Sr budget (Evans et al., 2001). They also facilitate the supply of atmospheric CO_2 via metamorphic decarbonation (Evans et al., 2008, Tiwari et al., 2016).

Apart from the orogenic setting hot springs can also be present in the areas of non-orogenic settings. In India, the tectonically active Himalayan terrain is considered as the orogenic provinces whereas the peninsular Indian region is referred as the non-orogenic provinces (Chatterjee et al., 2023). Considering both provinces, there are about 400 geothermal springs are found to be present in the Indian subcontinent (Chatterjee et al., 2023). The non-orogenic provinces are further divided into six sub-provinces namely, i) Cambay ii) Godavari iii) Sohana iv) Mahanadi v) Son-Narmada-Tapi, and vi) West Coast geothermal provinces. Very limited studies address the implications of west coast geothermal provinces (Chatterjee et al., 2023). Heat in these regions is supplied by the tectonic upliftment of hot basement rocks. It could be because of the deep circulation of water through the permeable zones created by folding or faulting (Nicholson, 2012). These can also release substantial amounts of CO_2 which has limited estimation.

Although basaltic lithology contains only 3.5% to 5% of the global land surface area (Hartmann and Moosdorf, 2012; Dessert et al., 2003) it contributes 30% of the CO_2 consumption of global silicate weathering (Dessert et al., 2003; Gaillardet et al., 1999). Despite having limited lithology coverage globally, basaltic lithology shows a significant contribution in providing weathering flux into rivers flowing through such lithology because of the faster weathering rate (Gislason et al., 1996; Louvat and Allegre, 1997, 1998; Gaillardet et al., 1999; Dessert et al., 2003; Schopka et al., 2011). Also, the regions that are dominated by Ca-Mg

silicate lithology having high precipitation and relief are the major regions of CO_2 sink on land (Gislason et al., 1996). The Deccan volcanic province (DVP) is one of such region in India that receives intense rainfall because of the orographic barrier of the western ghat. This leads to high stream power of the river basins in this region and hence enables them for higher erosion.

Das et al., (2005) provided an estimation of area-averaged CO_2 consumption rate (3.6×10^5 mole/km^2/yr.) and CO_2 drawdown (1.8×10^{11} mole/yr.) in Deccan basalt by silicate weathering which is ~ 1.5% of the total CO_2 consumption by continental silicate weathering. Apart from the consumption, there are sources of CO_2 via hot springs which is less studied in this region. DVP of India provides an appropriate location for investigating the geochemical behavior of hot springs and their role in supplying atmospheric CO_2. These hot springs lie along a liner belt in the west coast geothermal province (WCGP) (Chandrasekharam, 2000). There are about 60 geothermal springs distributed in 18 locations of the west coast geothermal province (Chandrasekhar et al 2018). These geothermal springs are parallel to the west coast which covers a linear distance of ~ 350 km and most of these springs are passing into the adjacent rivers. Hence, it is also crucial to estimate its solute flux influence on associated river and adjacent groundwater of the region. Few studies exist on the Deccan hot spring which estimates its solute sources, reservoir temperature, energy generation, and water-rock interaction (Ansari et al., 2014; Chandrasekhar et al, 2016, 2018; Gurav et al., 2016; Chatterjee et al 2017; Chandrasekharam et al., 2000; Ansari et al., 2014; Chatterjee et al., 2000; Reddy et al., 2013; Muthuraman, 1986). Furthermore, there exists a number of studies that documented the moisture sources of these thermal springs using oxygen and hydrogen isotopes as proxies and found it to be primarily of meteoric origin (Minissale et al., 2000, 2003; Singh et al., 2014; Gurav et al., 2015). Chandrasekhar et al., (2018) gave a conceptual model for the Deccan hot springs and the reservoir depth of the hot springs are about 2000 m having an average thermal gradient of 55˚ C/km. They also suggested the involvement of marine sediments in two of the hot spring using $\delta^{11}B$ as a proxy. Based on major and trace element behavior of geothermal springs, Gurav et al., (2015) proposed, that the northern group of hot spring have signature of seawater mixing whereas southern group of hot springs are circulating through basement granite. Chatterjee et al., (2017) adopted a multi-isotope approach to evaluate the water and solute sources in Tural and Rajwadi hot spring. $\delta^{13}C$ value (ranges from -19.62 to -20.10 ‰) of DIC suggests the CO_2 in these two hot springs is sourced from silicate weathering and decomposition of organic matter of C_3 type of vegetation. $\delta^{34}S$ value (range: +19.6 to 20.43 ‰) of the sulphate dissolved in water suggests the water is sourced from marine origin which

could be due to the entrapment of paleo sea water in sedimentary lithology. $\delta^{11}B$ (range: +34 to +41‰) also suggested a marine water and silicate weathering is the possible solute source of the hot spring. ^{222}Rn concentration of the Tural hot springs varies from 1087 ± 132 to 1655 ± 177 Bq/m^3 whereas for Rajwadi it varies from 152 ± 67 to 350 ± 82 Bq/m^3 (Ansari et al, 2014). Based on this observations they emphasized the hydrogeological control and deeper heat source of the hot spring.

Minissale et al., (2000) revealed the deep circulation of meteoric water with some local mixing of connate and marine water from the fluid chemistry and the large He concentration as gas phase. Reddy et al., (2013) dated the age of the Tural and Rajwadi hot spring water and showed the radiocarbon age of the Tural hot spring water (3080 ± 40 years BP) is relatively more than the Rajwadi hot spring (1720 ± 45 years BP). In addition, geophysical study by Low et al., (2020) suggested, the Tural and Rajwadi hot spring water circulates through cross-cutting lineaments which serves as a conduit for the circulation. These lineaments are characterized by faults and extend to a depth of very shallow (~<50-150 m) to deep (~50-500m) within the basalt flow (thickness:770-800m). Singh et al., (2014) also proposed the granite batholith extending from Gugi to Rajapur provides radioactive heat to the Rajapur thermal spring.

The geothermal potential of the WCGP hot springs (Unhavre-Farare, Tural and Rajwadi) are found to be a probable site for the exploration of medium enthalpy geothermal resources (Chandrasekhar et al., 2016).

However, the study of these hot springs in the context of solute fluxes to the river and their CO_2 release rate is less studied, particularly in the Deccan region. In this study, efforts are made to compute the solute fluxes of hot springs and adjacent rivers to the Arabian Sea. Also, the CO_2 release rate has been quantified using major ions data.

2 Chapter 2

2.1 Geological Background

One of the notable geological events that happened in the Indian plates' geological history was the formation and evolution of the Deccan Volcanic Province (DVP). This is considered one of the global interests of research particularly in the context of the formation and disintegration of the southern Gondwana landmass, the upliftment of the landmass, the eruption of magma in the deep mantle, the evolution of biotic species during that time, and climate change perspective. (Courtillot,1990; Khosla and Sahni,2003; Subbarao and Courtillot,2017). This is considered to be one of the most voluminous large igneous provinces (LIP) which produced a massive eruption of tholeiitic-type magma within a very short period (K-Pg Boundary) (Chent et al., 2007,2009). Being positioned close to the Cretaceous-Palaeocene boundary this event is assumed to be one of the major factors in the extinction of biotic mass at K-Pg boundary.

The DVP is one of the largest flood basalts in the world, spanning the northwest, central, and southern Indian Peninsula over 5,00,000 km^2 and is also possibly extended another 10,00,000 km^2 area beneath the Arabian Sea (Sen et al.,2001; Colleps et al.,2021; Jay and Widdowson.,2008). The varying degree of lava thickness is seen in the Deccan region which ranges 200 m or less in the east to 1.5 - 2 km in the west.

Deccan basalts are comprised of tholeiitic-type basalt which includes mostly phenocrysts of plagioclase, clinopyroxene-altered olivine, many opaque minerals, and altered glass (Beane et al 1986). Based on field, geochemical, and paleomagnetic evidence (Beane et al., 1986; Cox and Hawkesworth, 1985; Mitchell and Widdowson, 1991), it is concluded that the overall stratigraphic division of DVP consists of three subgroups and twelve formations, with a maximum thickness of approximately 3400 m (Mahoney et al., 2000).

The five formations are Bushe, Poladpur, Ambenali, Mahabaleshwar, and Panhala (from base to top; Fig. 1).

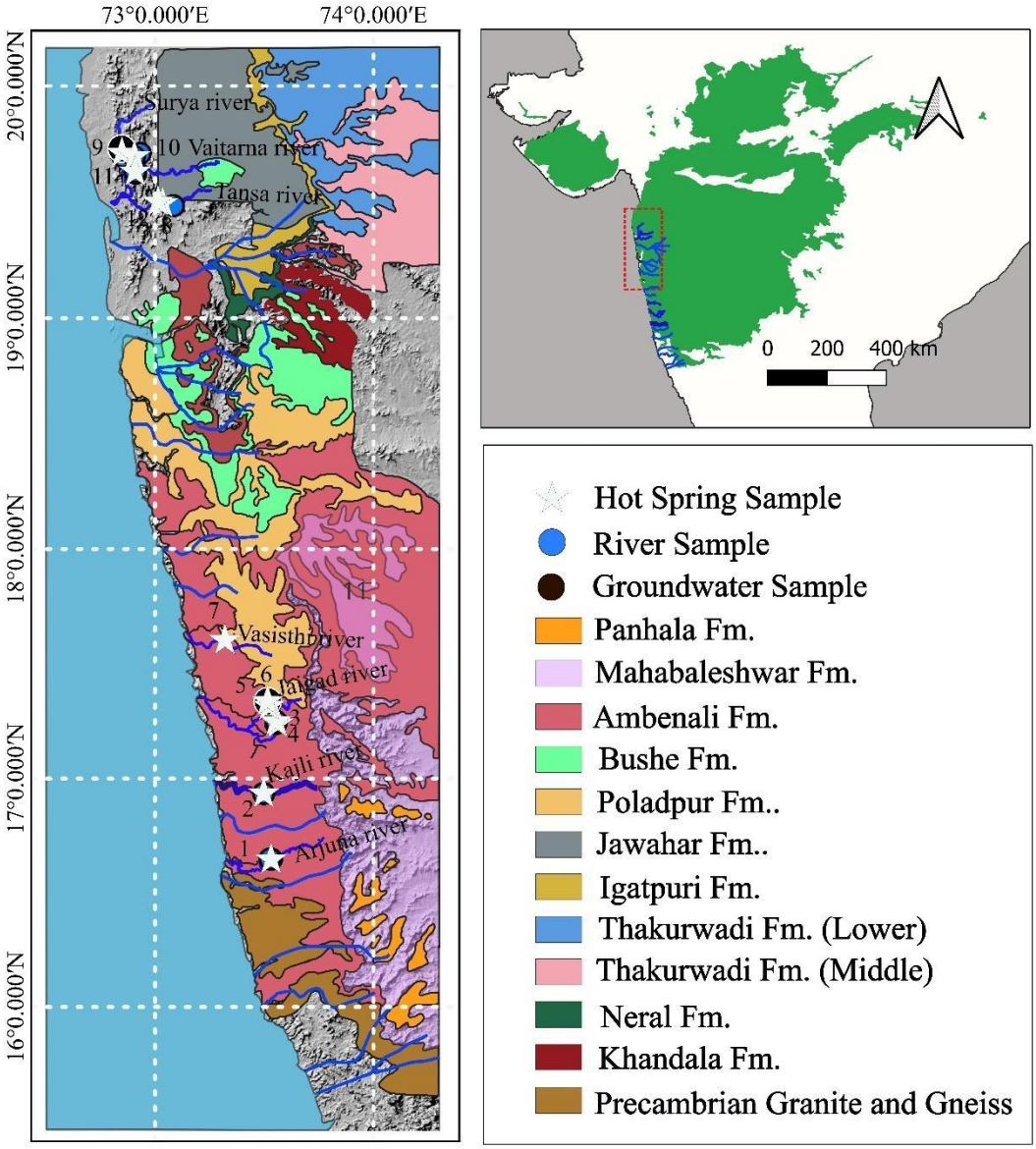

Fig.1: Location map of the hot springs from the Deccan traps, India; sample Id are given in table 3. Lithological details are modified after Chandrasekhar et al., 2018.

Numerous N-S, NE-SW, and NW-SE, trending lineaments have been found in the zone between the Western Ghat escarpment and the Arabian Sea. These lineaments are characterized by fracture zone, faults, and dykes (Desai and Bertrand,.1995). Some of these extend from 10 km to 100 km. Tectonics and the evolution of these structures have been studied extensively (Dessai et al.,1995; White and McKenzie,1989; Das and Ray (1983,1987)).

The Indian plate started its northward journey after its separation from Gondwanaland during the late Jurassic time and then subsequently it separated from Madagascar during Turonian-

Santonian times (94 - 83 Ma), followed by a detachment of Seychelles in Campanian-Early Maastrichtian times (Pande et al., 2017). India kept on moving northward until it collided with the Eurasian plate (Garzanti and Hu, 2015). Although volcanism happened in the Mid to Late Deccan volcanic province signifies one of the eruptions of basaltic lava onto the Indian continental mass when it passed over the Reunion hotspot between 68 Ma and 62 Ma (Kale et al.,2020) .

During the separation of the Indian plate from Seychelles, a major faulting event took place parallel along the west coast margin (trend NNW-SSE) known as the west coast fault (WCF) (Crawford et al., 1971; Mahoney et al., 1988). The formation of Panvel flexure is also associated with the WCF which could be formed due to extensive extensional stress created during the rifting (Dessai et al., 1995; White and McKenzie, 1989). Numerous dyke swarm was intruded in between the extensional N-S fracture system caused by this lithospheric extension created during the separation of India Seychelles (White and McKenzie, 1989) . Das and Ray (1983, 1987) suggested that the axis of this Panvel flexure continued up to Rajapur in Ratnagiri district. The continuation of Deccan traps up to offshore and the existence of a seaward dipping fault system in offshore is also confirmed by the seismic reflection study (Hinz and Closs, 1969) and the drill hole data of ONGC India. Also study done by Saha et al., (2023) reported the presence of plume-related long-lived sulfide melt at a depth of 50-60km and 90-110 km in the western segment of Deccan. They have also reported a low velocity (3.3-3.5 km/S) layer in the shallower crust (8-17 km depth), interpreted as an elongated frozen magma chamber. There is also evidence of basaltic mafic intrusion which is responsible for producing massive CO_2 degassing (Saha et al., 2023).

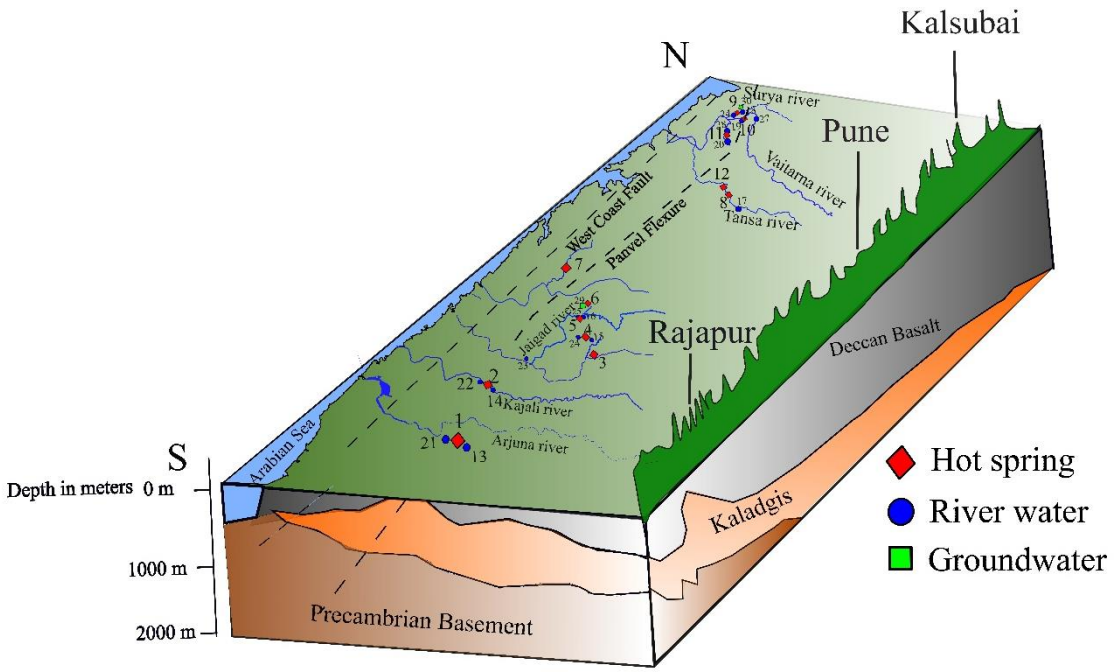

Fig. 2: Schematic block diagram showing sampling location of hot spring, river, and groundwater samples; modified after Chandrasekhar et al., 2018.

Thermal springs are restricted to the area along India's west coast (N-S), following this NNW-SSE trending lineament in the western part of the Deccan because of the high heat flow in this region. In our study area of the west coast geothermal province, geothermal springs extend linearly from Koknere (17˚20'13.49"N,73˚30'55.06"E) in the extreme north to the Rajapur hot spring(16˚38'44.28"N, 73˚31'52.16"E) in the extreme south running parallel to the west coast fault(Chandrasekhar et al.,2016). Along our study region, the thickness of basalt varies from approximately 600 m to a maximum of about 2500 m. Basaltic lava flows near the Tural-Rajwadi hot spring show pahoehoe in nature with the secondary mineral deposition of calcite, nontronite, clinoptilolite, stilbite, apophyllite, cristobalite, etc. (Monterio et al., 2019). The North-South cross section of the Deccan volcanic flow (Subbarao et al., 1994) indicates that the flow thickness decreases as they approach Rajapur on the southern edge, where they are visible on top of the Precambrian basement. On the southern side of the DVP Precambrian gneissic and granitic basement and associated quartzites occur as inliers in many places (Ramanathan and Chandrasekharam, 1997). Also, in the nearby area of Math and Rajapur, Kaladgi sedimentary rocks have been found as inliers which explains the resistivity contrast in the southern region of DVP (Arora, 1986). This area has an average geothermal gradient of 57°C/km (Chandrasekharam, 2000), and heat flow value varies in between 45 ± 10 mW/m^2 (Roy and Rao, 2000).

2.1.1 Geohydrology

The rocks that are important in retaining water in this region are basalt (Upper Cretaceous to Lower Eocene age), laterite (Pleistocene), and alluvium deposit (Recent). These are not very permeable due to the lack of interconnection between vesicles and secondary mineral deposition inside the vesicles of Deccan basalt. But in this region, secondary porosity is produced due to the cooling joint's partition planes, cracks and fissures, fractures, and faults. Here the aquifers are of two types, one which is shallow remains in unconfined conditions, another is deep aquifers that remain in semiconfined to confined conditions (Chatterjee et al., 2017). The groundwater level varies from 10 m below ground level (bgl) in the shallow aquifer to 10-20 m bgl in the deep confined aquifer during the pre-monsoon time. During the post-monsoon, the water table comes up to less than 5 m bgl in the shallow aquifer and 10-20 m bgl in the deeper aquifer (Chatterjee et al., 2017; CGWB, 2004).

2.1.2 Climate

The study area experiences the maximum rainfall during the south-west monsoon season (Sarker et al., 1966; Grossman & Durran 1984). The rainfall amount is higher near the escarpment (2000 m/yr), which starts to decrease as we move toward the Deccan plateau (<1000 mm/a; Tawde and Singh, 2014). The Western Ghat plays an important role in controlling geo-hydrological and climatological parameters. It acts as an orographic barrier for the precipitation of southwest monsoon. In the western ghat region mean annual temperature is 27 °C and varies from 11°C to 23°C from south to north (Reddy et al., 2019). Major rivers which originate from the Western Ghats flow both in easterly and westerly directions. Westerly flowing rivers experience tropical wet and highly humid climates.

3 Chapter 3

3.1 Materials and Method

Figure 3 depicts the analytical methods adopted during this study.

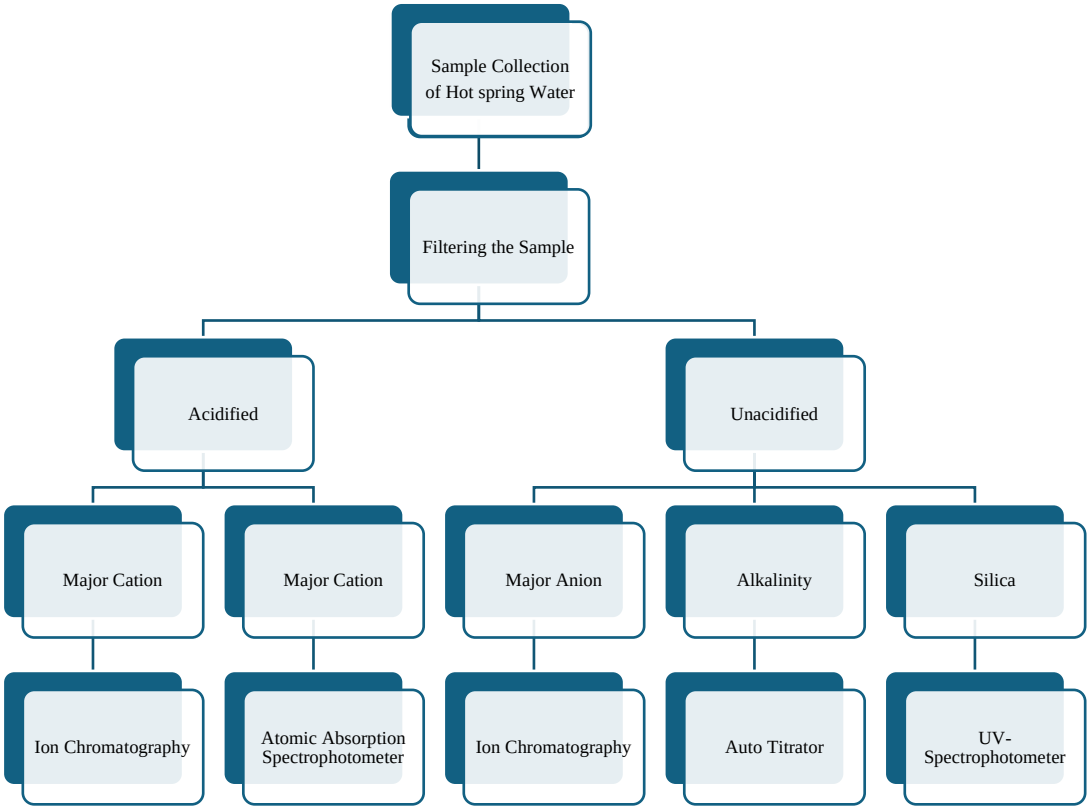

Fig. 3: Flow diagram for analytical techniques followed in this study.

3.1.1 Sample Collection and processing.

Water samples from the hot spring, river, and groundwater were collected along a linear stretch in the west coast geothermal province. A total 29 samples (12 hot springs, 16 rivers and 2 groundwater) were collected in this field trip conducted in October, 2023. Samples were collected in pre-cleaned polypropylene (PP) bottles, after rinsing the bottles with ambient water at least three times. Two liters of samples were collected during the field and properly sealed with teflon tape to avoid any leakage during transportation to the IISER Pune. All the samples were filtered using 0.2 µm nylon filter paper to filter all the suspended load from the samples and filtered samples were transferred into new bottles and stored for analysis. Two separate aliquots (of 500 ml volumes) of filtered water samples were taken; one was acidified using HNO_3 to make the pH of the samples lower than 2 for the measurement of cations (Na, K, Ca, and Mg). The unacidified aliquot was used for the measurement of anions (F, Cl, NO_3, SO_4, and HCO_3).

3.1.2 Onsite Measurement

The geographical latitude, longitude, and altitude of the sampling sites are obtained from a portable Gramin Global Positioning System (GPS). pH and temperatures of each sample were measured on-site using a portable probe (Hanna Instruments; HI98128 sensor). Before going to the field every time this instrument was calibrated using a buffer solution (pH of 4, 7 and 9.2).

3.1.3 Geochemical Analysis of Water Samples

3.1.3.1 Alkalinity Measurements

Alkalinity of the samples was measured using an auto-titrator (Methrohm Titrino Plus 877) by acid-based titration method with 0.01 N diluted HCl. Before the experiment instrument probe was calibrated using buffer solutions of known pH (of 4,7 and 9.2).

3.1.3.2 Major Ion Analysis

Major ions (Na^+, K^+, Ca^{2+}, Mg^{2+}, F^-, Cl^-, NO_3^-, SO_4^{2-}) of these samples were measured using Ion Chromatography (Metrohm Compact IC Plus 882) . For some hot spring samples K and Mg were measured using Atomic Absorption Spectrophotometer (AAS). ICP multi-element standards of known concentrations were used for making standards for cation and anion measurements respectively.

The average error for all the analyses is 2% (Table 6). Measured and expected concentrations of the known for major ion and silica showed a good correlation (r^2 = 0.9965) between the measured and expected concentrations which are shown in Fig. 4 and Fig. 5

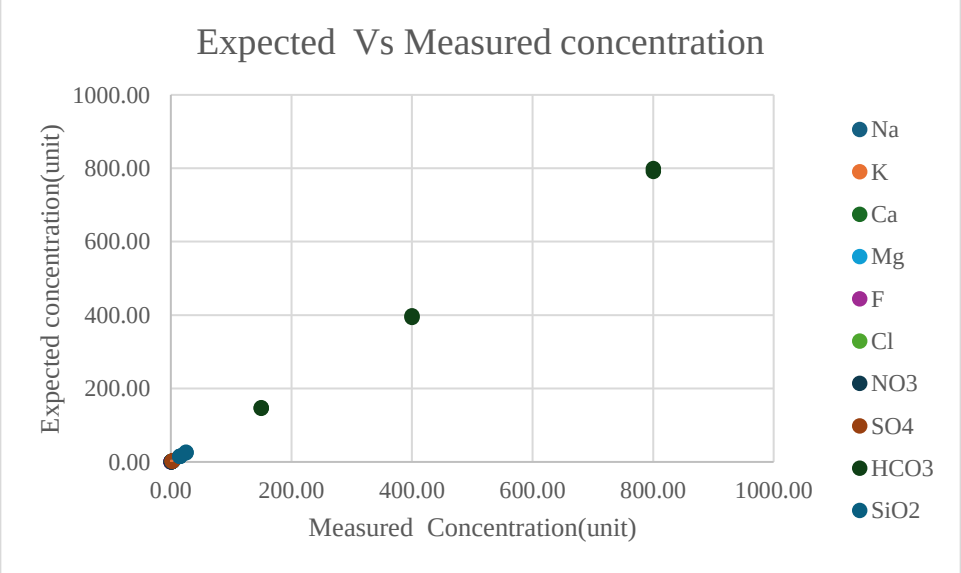

Fig 4: Plot of expected vs. measured concentration (ppm/µM) of different major ions.

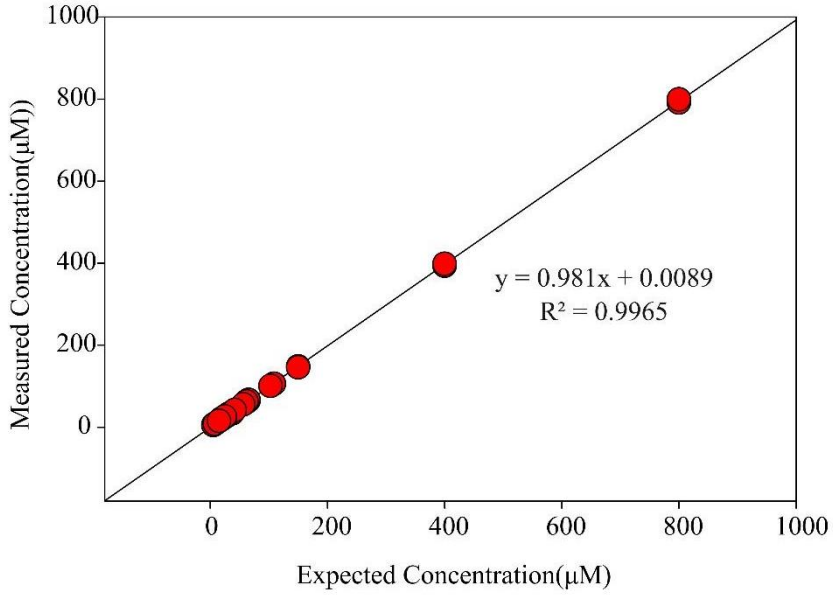

Fig5: The plots showing the expected and measured concentration of all chemical species during the analysis. The positive correlation signifies accuracy and precision of the analysis.

Repeat measurements of some samples were also conducted to constrain the precession of these analyses.

Average precision for all the measurements was 2% (Table 6). Replicate analysis of some previously measured sample and published data samples were also measured to obtain the precision. Normalized inorganic charge balance (NICB = $[(TZ^{+} - TZ^{-})/ ((TZ^{+} + TZ^{-})/2)] \times 100$; where TZ^{+}(total cation) and TZ^{-}(total anion) are in Eq units respectively) for most (26 out of 28) of the samples, were within 10 %. The average NICB (Table 3) of the samples was ±6% (n=29) which confirms good data quality and suitable analytical methods followed. Calcite Saturation Indices (CSI) for all the samples were calculated from the major ion data using PHREEQC Software.

3.1.3.3 Dissolved silica measurements

For the measurement of Dissolved silica, UV Spectrophotometer (Cmdt International) was used. For this, the absorbance of the molybdenum-blue complexes formed by the samples were quantified. Accuracy of the analysis was monitored by measuring standards of known concentration and has been found with an average value of 4 %. Precision of the instrument were quantified by doing repeat analysis of samples and found to within 1 %.

4 Chapter4

4.1 Result

Chemical data for hot springs (n = 12), rivers (n = 16), and groundwater (n = 2) samples are provided in Table (3).

The temperature of the hot spring samples varies from 34 to 60°C (Average 45 ± 7°C, n = 12), which are higher than that observed for river (32 ± 4 °C) and groundwater (32 ± 1°C). The pH values of hot spring (8.09 ± 0.58), river (7.48 ± 0.63) and groundwater (6.78 ± 0.3) samples show wide variation. The TDS of the hot springs varies between 427 mg/L and 8137 mg/L with an average value of 1833 ± 2184 mg/L. This average value is about 6 -7 times higher than that observed for the river (264 ± 481 mg/L) and groundwater (248 ± 118 mg/L) samples.

The Na concentrations of the hot springs vary between 3410 μM and 46516 μM (avg. = 16152 ± 11708 μM, n = 12). This average value of Na is similar to that reported for Himalayan hot springs (Becker et al., 2007; Tiwari et al., 2016) and ~ 4 times lower than the Global average value (avg. = 63553 ± 176904 μM, n = 651; Tamburello et at.2022; Nicholson, 2012; Kaasalainen & Stefánsson 2012; Du et al.,2004). K is varying between 107 and 483 μM (avg. = 250 ± 112 μM). The Global averaged K value (3317±9325 μM; Tamburello et at.2022; Nicholson, 2012; Kaasalainen & Stefánsson 2012; Du et al., 2004) is ~ 13 times higher than the measured K value. However, Himalayan hot spring samples (1963 ± 3087 μM, n = 49) show ~ 8 times higher concentration than the measured K value. Ca concentration of the measured sample varies from 221 μM to 45792 μM with an average value of 6430 ± 12658 μM whereas the Mg concentrations is in the range of 4 μM to 308 μM (average: 73 ± 102 μM; n =12).

For the river water samples, Na ranges from 153 to 23093 μM (avg.= 2133 ± 5795 μM, n=16), K ranges from 10 to 515 μM (avg.= 59 ± 135 μM, n =16), Ca varies from 171 to 992 μM (avg. = 408 ± 258 μM, n=16) and Mg varies between 82 and 2938 μM (avg. = 408 ± 689 μM; n=16). The average concentration of Na is ~ 9 times, Mg is ~ 3 times, and K is ~ 2 times higher than the global river average (global avg. = Na: 244 μM, K: 36 μM, Ca:351 μM, and Mg:143 μM; Tripathy and Das., 2014).

Measured cations in the groundwater samples (n = 2) are Na (663 - 1518 μM, avg. = 1090 ± 604 μM), K (27 μM), Ca (192-1137 μM, avg.= 664 ± 668 μM), Mg (115 - 577 μM, avg.= 346 ± 327 μM).

The major anions for the hot springs samples are dominated by Cl^- (400 - 141263 μM) ions. Sub-ordinate concentrations of HCO_3 (184 - 4640 μM), SO_4 (47 - 1878 μM), NO_3 (14 - 697 μM) and F (51 - 311 μM) are also observed for the hot springs. The average HCO_3 concentration (848 ± 1222 μM; n = 12) is about an order of magnitude lower than the Himalayan hot spring (avg. = 7390 ± 8614 μM, n = 49), and the global average value (avg. = 10694 ± 5201 μM, n = 651; Tamburello et al., 2022; Nicholson, 2012; Kaasalainen & Stefánsson 2012; Du et al., 2004). The average SO_4 concentration of the samples is 1125 ± 531 μM (n=12). The concentration is comparable to that reported for the Himalayan hot springs (1461±2627 μM, n=49; Becker et al., 2007; Tiwari et al., 2016), but lower than the global average SO_4 value (10575 ± 55604 μM, n = 651; Tamburello et al., 2022; Nicholson, 2012; Kaasalainen & Stefánsson 2012; Du et al., 2004) for hot springs. The measured NO_3 value (275 ± 252 μM, n =12) is ~ 6 times higher than the Himalayan NO_3 (48 ± 88 μM, n = 49) and ~ 32 times lower than the global average value (avg. = 8924 ±19295 μM, n=651). The average value of F is 151 ±69 μM which shows a similar concentration value with the Himalayan hot spring (avg. = 189±227 μM, n = 49) but ~ 2 times lower concentration than the other peninsular hot spring (avg. = 331 ±300 μM, n = 56).

For the river water samples (n = 16), F concentrations range from is 3 to 120 μM (avg. = 16 ± 29 μM), Cl values range from 86 to 31069 μM (avg. = 2534 ± 7763 μM), NO_3 varies from 6 to 40 (avg. = 15±9 μM), SO_4 varies from 17 to 1372 μM (avg. = 162 ± 366 μM) and HCO_3 varies between 709 μM and 2373 μM (avg. =1314 ± 676 μM). When the measured anion value was compared to the Global average number (Tripathy and Das., 2014), the average Cl and SO_4 concentrations in these rivers are higher than the global average value (avg. = Cl: 144 μM; SO_4: 102 μM; (Tripathy and Das., 2014)

The concentrations of F (10 - 24 μM, avg. = 17 ± 10 μM), Cl (416 - 456 μM, avg. = 436 ± 28 μM), NO_3 (13 - 145 μM, avg. = 79 ± 93 μM), SO_4 (80 - 91 μM, avg. = 86 ± 7 μM), and HCO_3 (1547 ± 3650 μM, avg. = 2598 ± 1487 μM) show large variations in the two ground water samples.

The dissolved silica for the hot spring samples varies between 413 μM and 1521 μM. The average value of the dissolved silica is 1045 ± 307 μM (n=12) which is ~ 2 times lower than the Himalayan (2124 ± 1017 μM, n = 49; Becker et al., 2007; Tiwari et al., 2016), peninsular hot springs (1851 ± 446 μM, n=56) and ~3 times lower than the global average value (2921 ± 2800 μM, n=651; Tamburello et at.2022; Nicholson, 2012; Kaasalainen & Stefánsson 2012;

Du et al.,2004). Whereas dissolved silica for the river water samples (n = 16) varies between 359 μM and 1187 μM with an average value of 359 ± 1187 μM. The average concentration of dissolved silica in the global rivers (avg. = 127 Mm; Tripathy and Das, 2014) is ~4 times lower than the measured average value. In the groundwater samples dissolved silica (SiO_2) concentration ranges between 622 and 752 μM having an average value of 687 ± 92 μM.

5 Chapter 5

5.1 Discussion

5.1.1 Sources of solutes and origin of hot springs in the Deccan region

Chemistry of hot springs can provide clues about its solute sources and hence, can be used to understand subsurface interaction between rock and water. Solute concentration in the river and groundwater controlled by basin lithology. It, therefore, mainly supplied through weathering of silicate and carbonate rocks. The dissolution of gypsum and evaporite can also contribute solutes, mainly in the terrains with these lithological exposures. Additionally, anthropogenic inputs are another source of solute to river and groundwaters. Solute concentration in hot spring water is different from surface water because of its varied source of water. However, in hot springs sources of water could be of various origin. It can be a meteoric water source that can circulate deep in the crust up to a depth of a few kilometres through fractures and permeable zones and again come up to the surface. It can also be of connate water which remains in a trapped state in host sediment. It has also been suggested that water in hot springs can come from magmatic sources (juvenile water) and / or water derived from metamorphism (metamorphic water). Rock water interaction is considered to be the most dominant source of solutes in geothermal springs (Ellis and Mahon1964, 1967). Bischoff et al., (1981) have shown that seawater can also act as a solute supplier to the hot spring in the geothermal system of the coastal area. Because of density differences magmatic brine can mix with meteoric water deep below the crust. A small quantity from the magmatic brine can make a significant change in the solute concentration as these are rich in solutes/gases like Cl, SO_2 CO_2. Validation of such type of mixing processes can be traced from isotopic signatures.

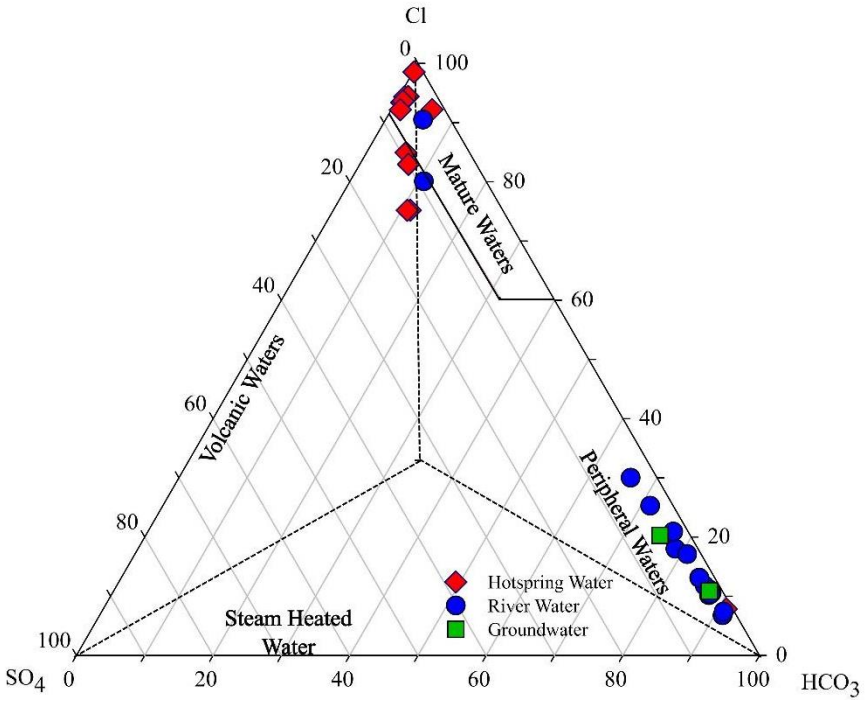

Fig. 6: The ternary diagram showing the Cl-SO_4-HCO_3 facies and possible water types (Giggenbach, 1991).

Water types such as volcanic water steam heated water, mature water, and peripheral water have been classified based on the relative proportions of Cl, SO_4, and HCO_3. If the hot spring waters are plotted in the peripheral field, it will indicate a mixing phenomenon with cold groundwater.

Figure 6 shows all the groundwater and river water samples, except for two river water samples, are falling in the peripheral water field. Hot spring water and few river water samples (n = 2) is showing the signature of mature water. This indicates two river water samples have a major confluence of hot springs. The appearance of the hot spring samples data in the mature field indicates Cl-rich fluid coming from a deep source. This plot also identifies waters that would be more appropriate for geothermometry. Sample points falling close to the Cl apex are most suitable for geothermometry (Nicholson, 2012). As the hot spring samples are falling in the Cl apex side of the triangle, hence it is suitable for geothermometry.

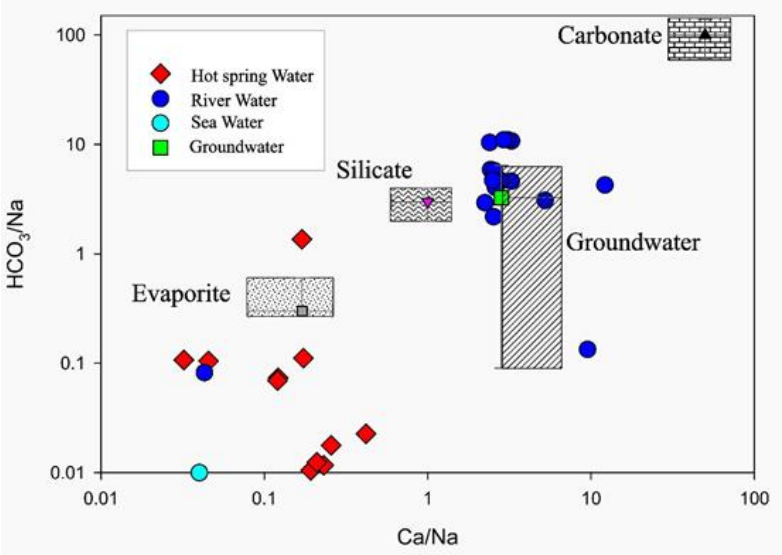

Fig. 7: Mixing plot showing the solute sources (endmembers of evaporite and carbonate are taken from Millot et al, 2003 and silicate end member is taken from Gaillardet et al., 1999)

Weathering dominance and water-rock interactions are mostly dependent on lithology. Lithological contribution can be interpreted from the mixing plot of Ca /Na and HCO_3/Na (Fig. 7). From the plot, it is evidenced that, all the river and groundwater samples (except two river water) are falling between silicates and carbonates end members. This indicates the source of solutes are from both silicates and carbonates, however, the contribution from the silicate is dominated. Whereas hot spring samples does not fall in the end member mixing regions. It might have gone through mixing processes of various water types. However, the mixing of seawater is the possible explanation as it falls near the seawater end member zone. Solute sources from evaporite sources can be discarded as there is no reported halite exposure in this area (Das et al., 2005).

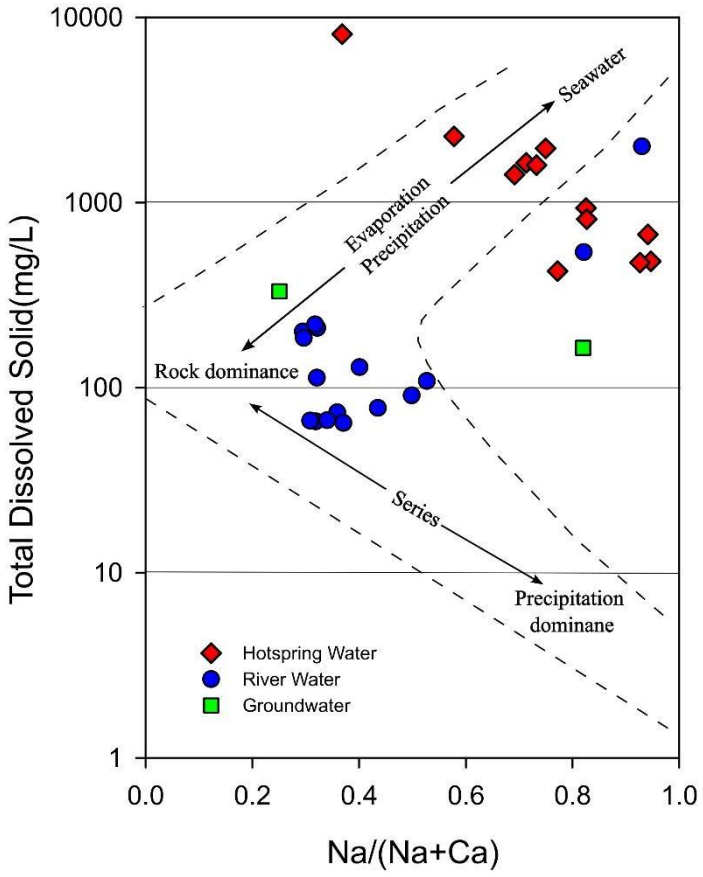

Fig. 8: Gibbs plot showing the Hot spring, river, and groundwater samples.

The molar ratio of Na and (Na+ Ca) are plotted against total dissolved solids (Fig. 8) to interpret rock, precipitation, and seawater dominance solute supply to the samples. Here the concentration of Na indicates the end member of saline water (eg. seawater), whereas Ca represents fresh water such as river groundwater. So marine contribution or atmospheric input of sea salt will increase the ratio [Na / (Na+Ca)] towards one but with different TDS values. From this plot (Fig 8) it is visible that hot spring samples are showing a trend of seawater dominance. Most (except two samples) of the river water are showing rock dominance which is contributing to the major solutes in the river water. Two of the river water samples are showing seawater dominance which can be due to the adjacent hot spring water confluence.

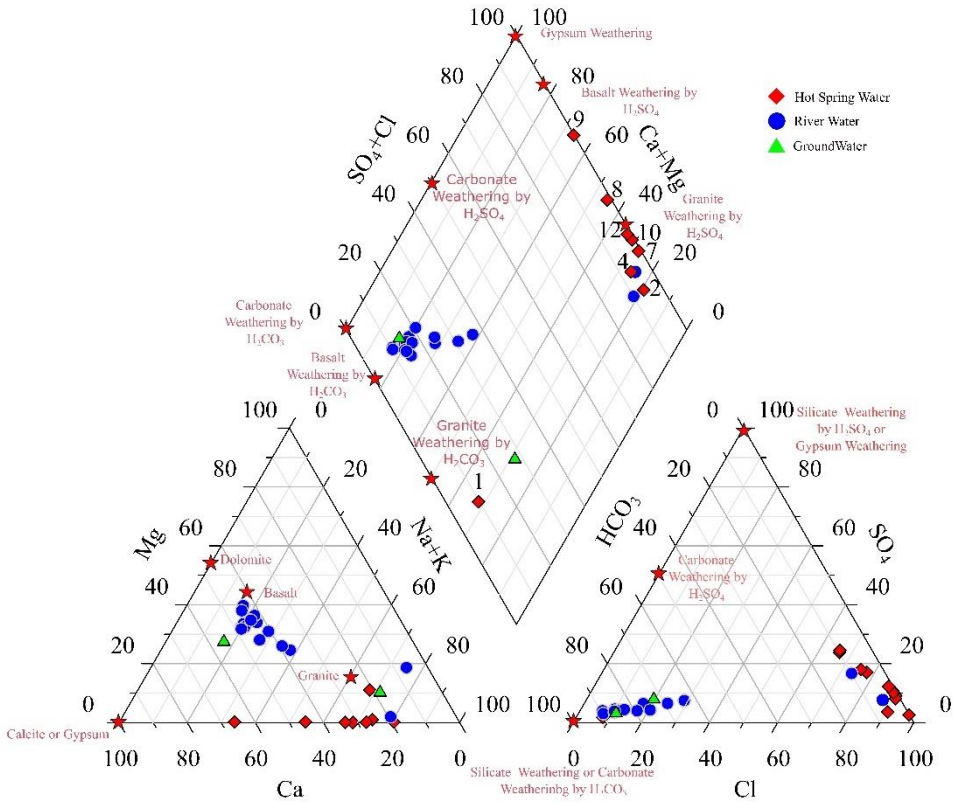

Fig. 9: Piper diagram for water chemistry data for the hot spring water, river water and groundwater samples (end members are from Spence & Telmer, 2005)

Graphical representation of Piper plot (Fig 9) gives an overview of the interrelationship between the cations (Na + K, Ca, and Mg) and anions (HCO_3, Cl, SO_4). The weathering of rocks of different end members with various natural acid-mediated weathering can be interpreted from this plot. Except for one hot spring, all the hot springs shows a trend of H_2SO_4 - mediated basalt weathering and H_2SO_4 mediated granite weathering. Only hot springs (#1) near Rajapur Unhale show H_2CO_3-mediated granite weathering. River waters are falling near the zone of basalt and carbonate weathering by H_2CO_3. One of the groundwater is showing the signature of basalt weathering whereas other one sample shows granite weathering. Most (except one) of the hot springs are of Na-Ca-Cl type. Rajapur -Unhale (#1) shows of Na-Ca-K-Mg-HCO_3 type character which is completely different from all the hot springs. This might be due to water sourced from a completely different reservoir. It is present in the southernmost part of the study area where basalt thickness is less, and also basement granite depth is shallower. Also, sporadic exposure of the Kaladgi group of rocks is present in the nearby area. Water may be circulating through the granitic and sedimentary siliciclastic as well as carbonate rocks.

The granitic rock contains 10 - 40% feldspar mineral albite in composition. Dissolution of Albite can produce Na and this might cause the enrichment of Na in Rajapur - Unhale thermal spring.

$$2NaAlSi_3O_8 \text{ (albite)} + 2H^+ + 9H_2O = 2Na^+ + Al_2Si_2O_5(OH)_4 \text{ (kaolinite)} + 4H_4SiO_4 \quad (1)$$

$$CaCO_3 \text{ (calcite)} + H_2CO_3 = Ca^{2+} + 2HCO_3 \quad (2)$$

$$Ca\ Mg(CO_3)_2 \text{ (dolomite)} + 2H_2CO_3 = Ca^{2+} + Mg^{2+} + 4HCO_3 \quad (3)$$

From the equation (2) and (3) it can be considered that the calcite and dolomite dissolution give a Ca/HCO_3 and $(Ca+Mg)/HCO_3$ molar ratio of 0.5 (Hann et al., 2013; Belkhiri and Narany,

a.

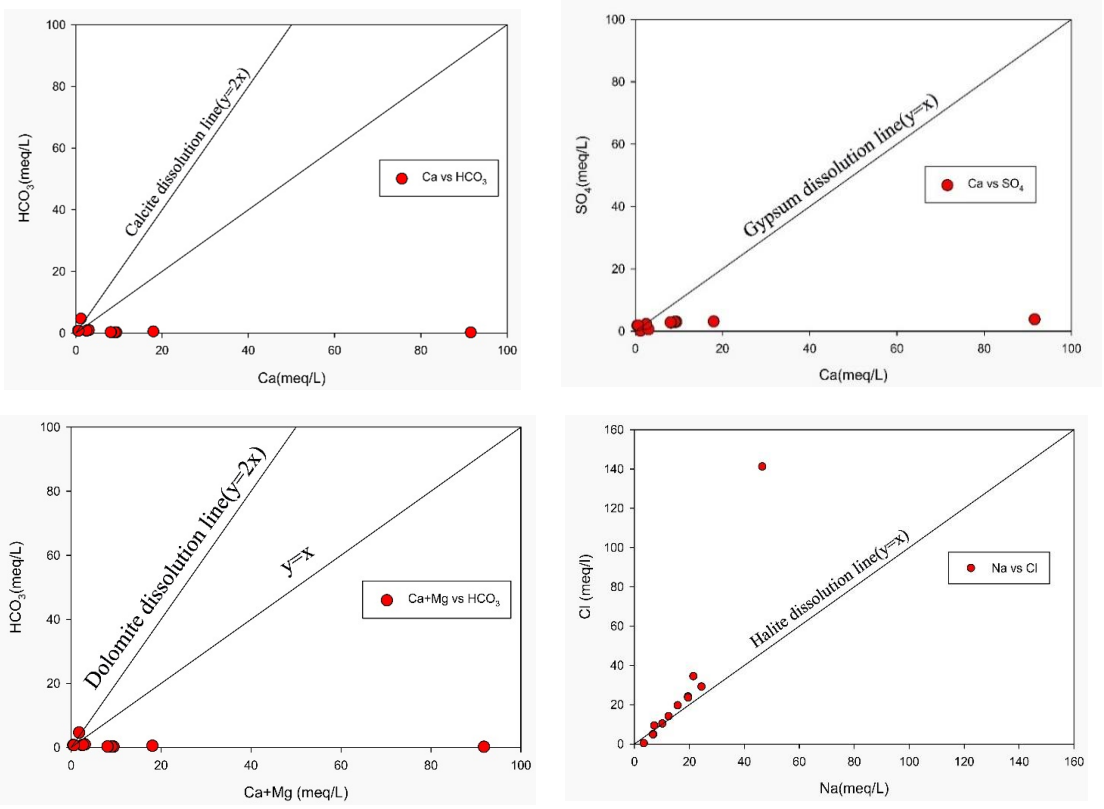

Fig. 10: Distribution of ionic ratios in the water samples of hot springs samples, a. HCO_3 vs Ca b.Ca vs SO_4 c. Ca + Mg vs HCO_3 d. Na vs Cl

2015). Except for three (#1, #5, #6), all the hot spring samples showed very high Ca/HCO_3 and $(Ca + Mg)/HCO_3$ molar ratio (Fig 10.1 c Table 9) which could be because of the dominance of Ca in basaltic lithology. Except for Rajapur Unhale (#1) Mg contribution is minimal in all other hot spring samples hence points to its insignificant contribution. Also Rajapur Unhale (#1) is showing a lesser molar ratio (molar ratio: 0.1) than produced by the dissolution of calcite. This also indicates less contribution of basalt (less amount of Ca) weathering in comparison to other hot springs. Fig 10.1 c shows all the river water samples are below the

dolomite dissolution line. Among the hot spring samples, one hot spring sample is above the dolomite dissolution line. Excess HCO_3 in the Rajapur-Unhale thermal spring might be a result of silicate weathering and a minor concentration of Ca can be because of ion exchange reaction. Whereas rivers before the confluence of hot springs and groundwater show a lesser molar ratio (river: 0.45 ± 0.03; GW: 0.33 ± 0.19) indicating higher HCO_3 contribution from silicate weathering. Fig 10.1.a shows some river water samples are falling on the calcite dissolution line indicate carbonate dissolution however hot spring samples fall below calcite dissolution line.

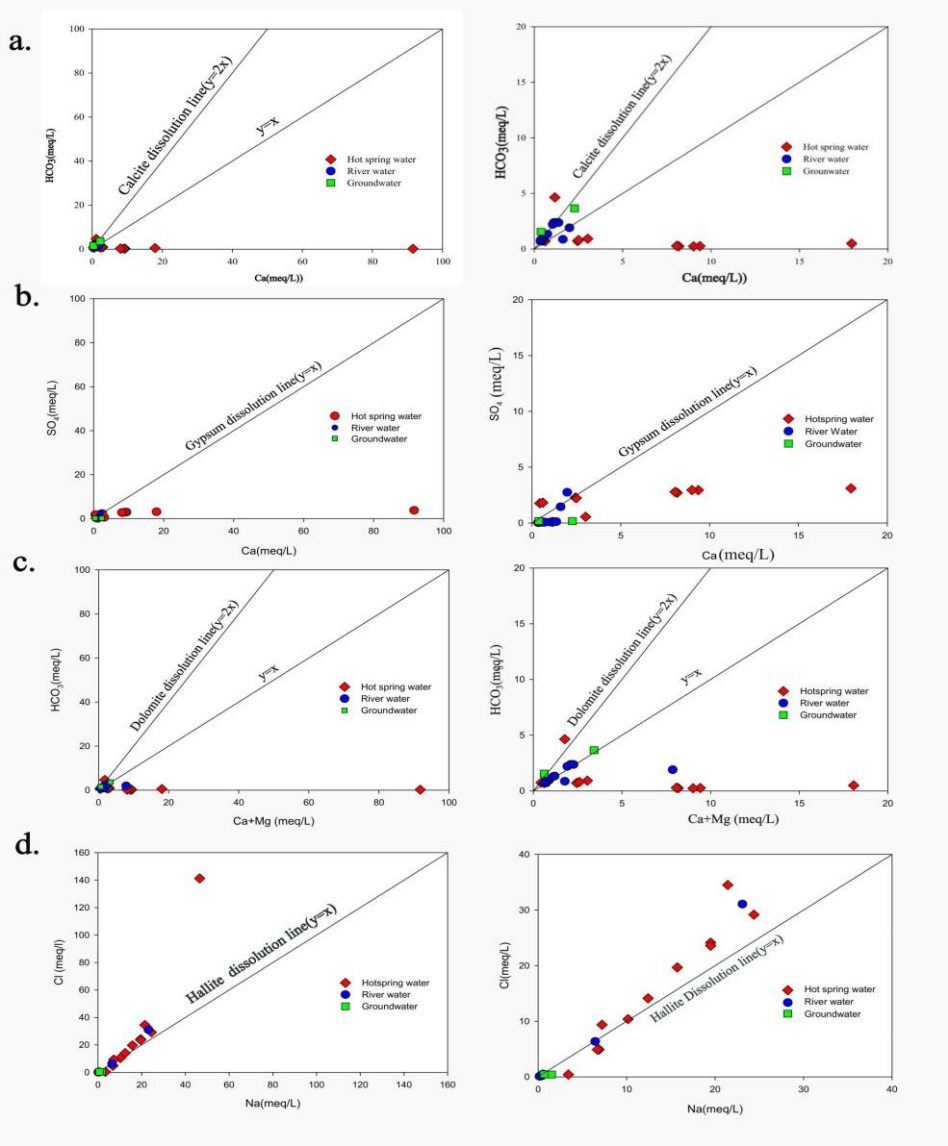

Fig10.1: Distribution of ionic ratios in the water samples of hot spring water, river water, and groundwater samples, a. Ca vs. HCO_3 b.Ca vs. SO_4 c. Ca+Mg vs. HCO_3 d. Na vs. Cl

Dissolution of halite produces Na and Cl in equal proportion and their molar ratio should be equal to 1 (Fig10.d). For our samples, Rajapur Unhale (#1) is showing a molar ratio of 9 which indicates an excess of Na in comparison to Cl (Table 9). Excess of Na could be due to water-rock interaction with basement granite. One of the hot springs is showing Na/Cl ratio near 1 which indicates a contribution from the dissolution of evaporite and the rest are showing Cl excess relative to Na (Fig10.1 d). One of the hot spring samples (#9) near Koknere is showing a very high excess chloride (Cl) relative to Na (Na/Cl molar ratio of 0.33) in comparison to the others. This is probably the highest reported Cl value in Indian geothermal spring water. Such type of Cl enrichment can happen due to contribution from the deep-level magmatic fluid as these types of fluids provide compounds like HF, HCl, SO_2, H_2S, and H_2O vapor which convert into NaCl complex interacting with the host rock and are released at the surface with hot spring water (Shah et al.,2019).

Precipitation and dissolution of gypsum produce Ca and SO_4 and the molar ratio between these two would be 1:1 (Fig. b). Most of the hot spring and river water are below the gypsum dissolution line (Fig10.1 b)

$$CaSO_4 + 2H_2O = Ca^{2+} + SO_4^{2+} + 2H_2O \quad (4)$$

If Ca, Mg, HCO_3, and SO_4 are sourced from the dissolution of carbonate and sulphate minerals from (Ca + Mg) and (HCO_3+SO_4) will show a 1:1 relationship and the sample points should fall on this line. If the points fall above the 1:1 line, then ion exchange might be the dominant process while data plotted below suggest the reverse of the ion exchange reaction (Das et al., 2021).

Ion exchange: $2Na - Clay + Ca^{2+} = 2Na^{+} + Ca - Clay2$ (5)

Reverse Ion exchange: $Ca^{2+} - Clay2 + 2Na^{+} = Ca^{2+} + 2Na^{+} - Clay$ (6)

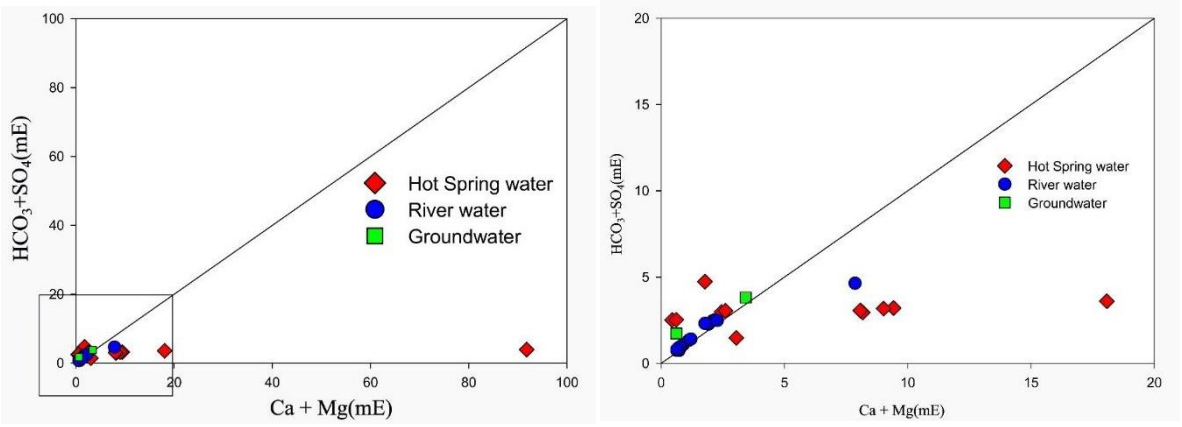

Fig11: The plot showing the HCO_3+SO_4 vs. Ca +Mg correlation for hot spring, river, and groundwater samples

The plot shows some of the hot spring samples fall above the 1:1 line suggesting the ion exchange reaction of Ca for Na decreased the value of (Ca+ Mg) overall. Five hot spring water and one river water sample are plotted below the 1:1 line indicating an increased number of Ca +Mg compared to HCO_3+SO_4. which can happen due to reverse ion exchange.

5.1.2 Geothermometry

Mahon (1966) established a relationship between dissolved silica concentrations and it's reservoir temperature. Later Fournier and other co-workers developed rigorous geothermometry relationship based on the solubility of silica species (Morey et al., 1962; Fournier,1966; Fournier and Marshall,1983) .

Reservoir temperature (T [$^{\circ}C$]) can be calculated by the following equation.

Quartz, no steam loss: $T(^{\circ}C) = \frac{1309}{sio_2\,]} - 273$ (7)

Quartz with maximum steam loss at 100 ˚C: $T(^{\circ}C) = \frac{1522}{sio_2\,]} - 273$ (8)

Where, SiO_2 is the concentration of silica. For applying a quartz geothermometer the temperature must be below 250 ˚C.

In high-temperature systems, Na, and K variation in geothermal waters happens due to the ion exchange of Na and K in co-existing alkali feldspar following the reaction below.

$NaAlSi_3O_8$ (Albite)+ K^+(aq) = $KAlSi_3O_8$(K-Feldspar) + Na^+(aq) (9)

Over experiment, geothermometry equations have been established by number of studies (Truesdell, 1976, Tonanani,1980; Arnorsson,1983; Fournier,1979; Nieva and Nieva,1987) which matches well to estimate the reservoir temperature in the range of 180 to 350 ˚C.

The reservoir temperature calculated for the hot springs is provided in Table 7. The average reservoir temperature for all the hot springs, calculated from the SiO_2 and Na/K geothermometer is 111 ± 14 ˚C and 128 ± 58 ˚C respectively. This estimated temperature is 1.4 times higher than the average Himalayan hot spring reservoir temperature (Avg: 80˚C ± 18 ˚C, silica geothermometer; Tiwari et al., 2016).

5.1.3 Solute fluxes estimation of hot spring and adjacent rivers

For the estimation of solute fluxes concentration value of different ions is multiplied by the discharge value of the river and hot spring (Table 5). Although the hot spring water has a very high concentration of solutes their discharge is very low. But in river water samples although solutes are present in a lower concentration their annual discharge is 10^4 orders higher than the hot spring samples (Fig.12). Because of this reason overall annual flux of river water is higher than the hot spring water. For the flux calculation, 5 samples of hot spring water and 7 samples of river have been considered.

Figure 12 shows, that among all hot spring samples HS23/07 is showing the highest annual Na, Ca, Cl, SO_4, and TDS flux because of higher discharge. The average Na flux of the hot spring sample is 3.49×10^6 moles/yr which is 2.53×10^2 times lower than the calculated river Na flux (average 8.83×10^8 moles/yr). For hot spring water average Ca flux is estimated as 6.78×10^5 moles/yr which is 1.42×10^3 times lower than the average flux of the river (average 9.62×10^8 moles/yr). Cl flux from the hot spring is calculated as 4.17×10^6 moles/yr and from the river is calculated as 5.62×10^8 moles/yr. For river water samples Cl flux is 1.35×10^2 times higher than the hot spring.

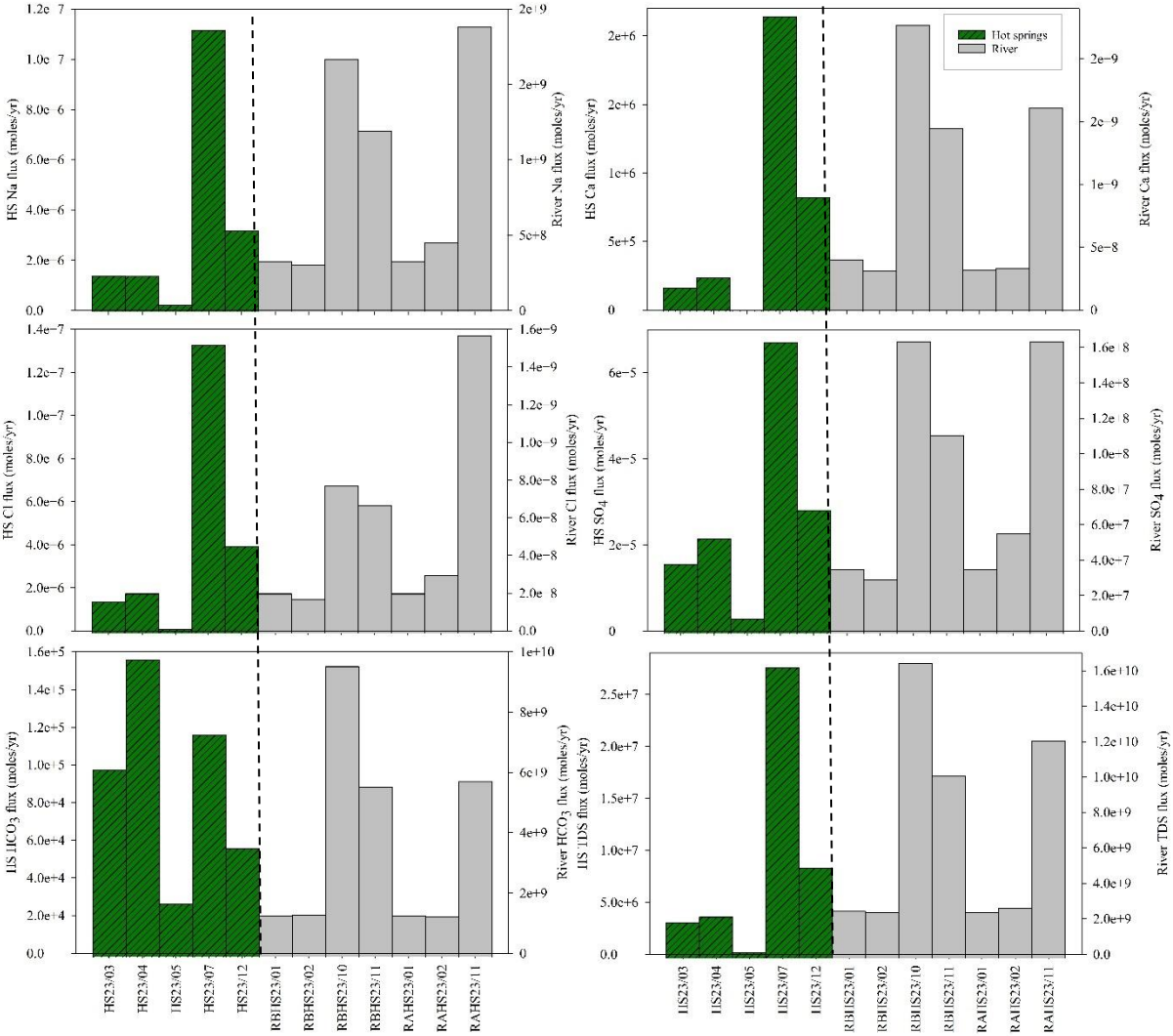

Fig12: The figure presents the fluxes of Na, Ca, Cl, SO_4 and HCO_3 fluxes of hot spring and corresponding rivers.

The average SO_4 flux value for the hot spring is 2.74 $\times 10^5$ moles/yr whereas in rivers it is 8.54 $\times$ 10^7 moles/yr. Riverine SO_4 flux is 3.12 $\times 10^2$ times higher than the hot spring flux. The river water average HCO_3 flux is calculated as 3.78 $\times 10^9$ moles/yr and hot spring water shows an average value of 9.17 $\times 10^4$ moles/yr. River water average value of HCO_3 is 4.12 $\times$ 10^4 times higher than the hot spring flux of HCO_3. The average TDS value of the hot spring and river are 8.87 $\times 10^6$ moles/yr and 7.08 $\times 10^9$ moles/yr respectively. The average TDS flux value of the river is 7.98 $\times 10^2$ times higher than the average hot spring value. Moreover, the elemental flux in river water in this study is found higher than the hot spring elemental flux because of the higher discharge in the river. However, if we consider the area of the hot spring or the volume

of the hot spring discharged water then it significantly contributes to providing solute supply to the ocean.

5.1.4 Estimation of CO_2 flux

Evans et al., 2008 proposed a direct method for calculating the CO_2 flux that is released from the hot spring. Bicarbonate ($HCO_{3)}$ data has been used as the total DIC of the sample. Multiplication of discharge data with the total DIC will give the value of CO_2 flux (Evans et al., 2004). Tiwari et al., 2016 proposed another approach for quantifying the CO_2 flux from the major ion data. Metamorphic CO_2 flux can be estimated by determining the total DIC concentration (C_{excess}) devoid of any DIC contribution from the water-rock interaction or dissolution of carbonate minerals. For calculating the C_{excess} the below mentioned equation is used:

$$C_{excess} = DIC \approx HCO_3^- - (Ca^{2+} + Mg^{2+} - SO_4^{2-}) \quad (10)$$

Ca^{2+} and Mg^{2+} indicate the mole that is coming from the dissolution of gypsum. Carbon can not come from the dissolution of gypsum, but Ca can be added, therefore SO_4 should be subtracted. Multiplying this C_{excess} with the discharge data will give the CO_2 release rate. Based on these two methods an attempt has been made in calculating CO_2 flux in Deccan hot spring samples.

Table1: CO_2 flux calculation from some selected hot springs of Deccan (method adopted from Evans et al., 2008; discharge data are taken from Chatterjee et al., 2016; Gupta and Sukija, 1974; GSI geothermal atlas of India, 1991).

Sl No	Sample Id	Location	DIC(m M/Kg)	Discharge (L/S)	Discharge (m^3/a)	Direct DIC Flux(mole/a)	CO_2 Flux(mole /a)
3	HS23/03	Rajwadi	0.7	4.5	1.403E+05	9.900E+04	9.900E+04
4	HS23/04	Tural	0.8	6.2	1.955E+05	1.572E+05	1.572E+05
5	HS23/05	Aravalli	0.7	1.2	3.784E+04	2.792E+04	2.792E+04
7	HS23/07	Unhavre-Farare	0.3	14.5	4.573E+05	1.173E+05	1.173E+05
11	HS23/11	Sativili	0.2	7	2.050E+05	4.968E+04	4.968E+04
	Sum					4.511E+05	4.511E+05

Table 2: CO_2 flux calculation from some selected hot springs in Deccan (method adopted from Tiwari et al., 2016; discharge data are taken from Chatterjee et al., 2016; Gupta and Sukija, 1974;).

Sl No	Sample Id	Location	C_{excess}(moles/L)	Discharge (L/S)	Discharge (L/a)	CO_2 Flux(mole/a)
3	HS23/03	Rajwadi	0.0006	4.45	1.40E+08	8.69E+04
4	HS23/04	Tural	0.0006	6.2	1.96E+08	1.22E+05
5	HS23/05	Aravalli	0.0014	1.2	3.78E+07	5.31E+04
	Sum					2.62E+05

Tural hot spring shows the highest CO_2 flux among all the hot spring samples and Aravalli shows minimum CO_2 flux (Fig. 13). The total CO_2 released from these hot springs is estimated to be 4.5 $\times 10^5$ moles / yr (Deccan sum1, Fig.14) which is 4.4 $\times 10^4$ times lower than the total sum of northwest Himalayan hot spring CO_2 release (2 $\times 10^{10}$ mole/yr) computed by Evans et al., 2008 (Fig14, Table 8).

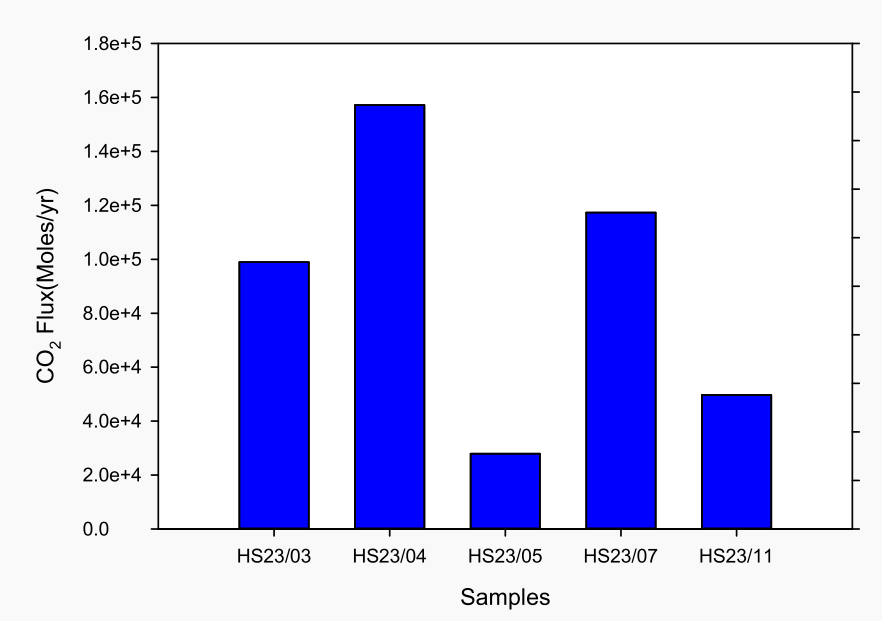

Fig13: Depicts the CO_2 flux of various Deccan hot springs. The CO_2 fluxes are estimated following an approach from Evans et al., 2008.

From the method given by Tiwari et al.,2016, the total CO_2 flux from the Deccan hot spring is calculated 2.62 $\times 10^5$ moles/yr (Deccan sum 2; Fig.14, Table 8). CO_2 release rate is computed from the Tural-Rajwadi hot spring by normalizing CO_2 flux by area and found as 1.708 $\times 10^8$

moles/km^2/yr. This value is about half of the CO_2 consumption rate (3.6 ×10^5 moles/km^2/yr) via silicate weathering for deccan region estimated by Das et al., 2005 (Fig.14 Table 8).

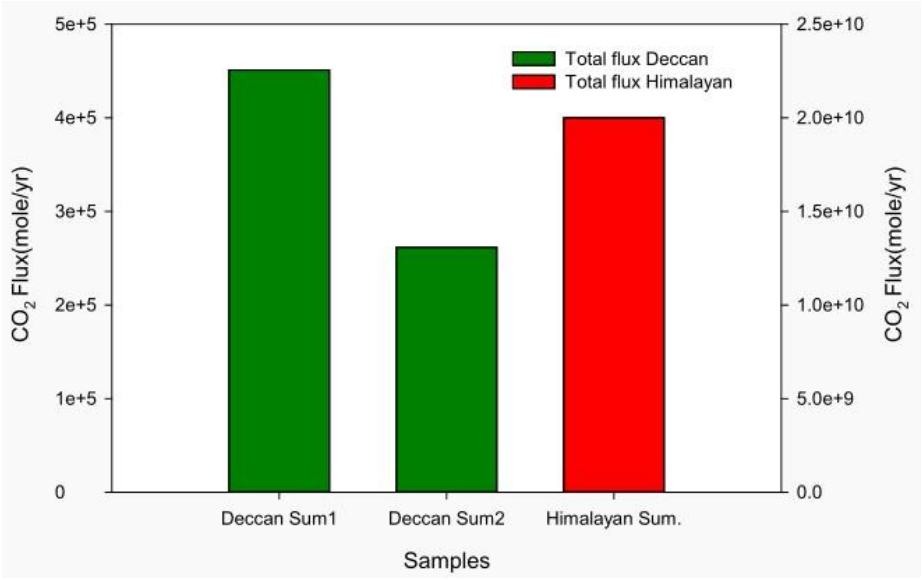

Fig14: Comparison of CO_2 flux of Deccan hot spring and NW Himalayan hot spring (Deccan sum 1 indicate the flux calculated by the method proposed by Evans et al., 2008 and Deccan Sum 2 indicate the flux calculated by the method proposed by Tiwari et al., 2016; NW Himalayan hot spring CO_2 flux data is taken from Tiwari et al., 2016.

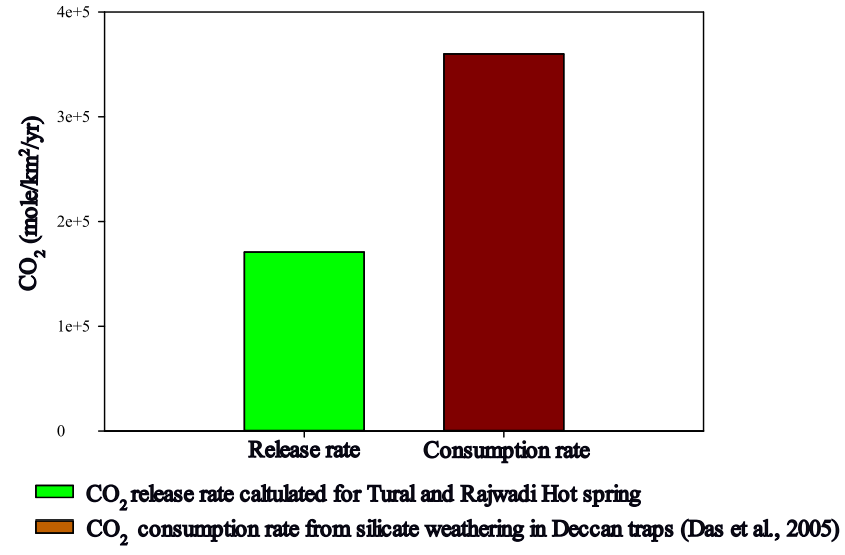

Fig15 : Comparison of CO_2 release rate calculated from Tural Rajwadi hot spring with the CO_2 consumption rate in Deccan via silicate weathering given by Das et al., 2005

6 Chapter 6

6.1 Conclusion

Although multiple evidence has emphasized the importance of the study of geothermal springs within the Indian subcontinent and in global studies, very sparse studies exist on hot spring contribution to the global carbon cycle and their elemental contribution to the global ocean. In this dissertation keeping this objective as goal, we have tried to identify the influence of hot springs through the following observations.

I. Solute sources for hot spring water indicate the Na-Cl rich water which might be a indicative of seawater mixing with meteoric water or dissolution of evaporite in the subsurface. For river water and groundwater the solute sources are mainly weathering of silicate(mainly basalt) and carbonate rock.

II. Among the hot springs one of the hot springs (Rajapur-Unhale is showing a completely different signature which is probably circulating through a different reservoir.

III. River water contributes more solute fluxes to the Arabian Sea due to its high discharge in contrast, hot springs supply lesser flux due to their low discharge and the dilution effect of the river.

IV. Average reservoir temperature for the Deccan hot spring is found to be 111 ± 14 ˚C to 128 ± 58 ˚C which is 1.4 times higher than Himalayan hot springs.

V. CO_2 release in the Deccan hot spring calculated from the direct method has been estimated to be 4.5×10^5 moles/ yr which is 4.43×10^4 times lower than the total sum of the release from the NW Himalayan hot spring (2×10^{10} mole/yr).

VI. About half of the CO_2 consumption in the Deccan region is counter balanced through CO_2 release rate of the adjacent hot spring.

Further study with more advanced isotopic analysis can be employed to better understand this process.

7 References

Ansari, M.A., Sharma, S., Kumar, U.S., Chatterjee, S., Diksha and Low, U., 2014. Hydrogeological controls of radon in a few hot springs in the Western Ghats at Ratnagiri district in Maharashtra, India. Current Science, pp.1587-1590.

Beane, J.E., Turner, C.A., Hooper, P.R., Subbarao, K.V. and Walsh, J.N., 1986. Stratigraphy, composition and form of the Deccan basalts, Western Ghats, India. *Bulletin of Volcanology, 48,* pp.61-83.

Belkhiri, L. and Narany, T.S., 2015. Using multivariate statistical analysis, geostatistical techniques and structural equation modeling to identify spatial variability of groundwater quality. Water Resources Management, 29, pp.2073-2089.

Becker, J.A., Bickle, M.J., Galy, A. and Holland, T.J., 2008. Himalayan metamorphic CO2 fluxes: Quantitative constraints from hydrothermal springs. Earth and Planetary Science Letters, 265(3-4), pp.616-629.

Bischoff, J.L., Radtke, A.S. and Rosenbauer, R.J., 1981. Hydrothermal alteration of graywacke by brine and seawater; roles of alteration and chloride complexing on metal solubilization at 200 degrees and 350 degrees C. Economic Geology, 76(3), pp.659-676.

Bob, M., Abd Rahman, N., Taher, S. and Elamin, A., 2015. Multi-objective assessment of groundwater quality in Madinah City, Saudi Arabia. Water Quality, Exposure and Health, 7, pp.53-66.

CGWB (Central Ground Water Board of India) (2014) Ground water in formation, Ratnagiri district, Maharashtra. 1825/DBR/2014, pp 1–21

Chandrasekhar, T., Chandrasekhar, V. and Chandrasekharam, D., 2016. Geothermometry of west coast geothermal province, maharashtra, India. Transactions of the 2016 Geothermal Resources Council, 40, pp.495-499.

Chandrasekhar, T., Minissale, A., Vaselli, O., Chandrasekharam, D. and Singh, H.K., 2018. Understanding the evolution of thermal fluids along the western continental margin of India using geochemical and boron isotope signatures. Geothermics, 74, pp.197-209.

Chandrasekharam, D., 2000, February. Geothermal energy resources of India-facts. In Proceedings Geothermal Power Asia 2000 Conference, Manila (pp. 12-19).

Chatterjee, S., Sharma, S., Ansari, M.A., Deodhar, A.S., Low, U., Sinha, U.K. and Dash, A., 2016. Characterization of subsurface processes estimation of reservoir temperature in Tural Rajwadi geothermal fields, Maharashtra, India. Geothermics, 59, pp.77-89.

Chatterjee, S., Ansari, M.A., Deodhar, A.S., Sinha, U.K. and Dash, A., 2017. A multi-isotope approach (O, H, C, S, B and Sr) to understand the source of water and solutes in some the thermal springs from West Coast geothermal area, India. Arabian Journal of Geosciences, 10, pp.1-11.

Chatterjee, S., Mishra, P., Bhushan, K.S., Goswami, P. and Sinha, U.K., 2023. Unraveling the paleo-marine signature in saline thermal waters of Cambay rift basin, Western India: Insights from geochemistry and multi isotopic (B, O and H) analysis. *Marine Pollution Bulletin*, *192*, p.115003.

Chenet, A.L., Courtillot, V., Fluteau, F., Gerard, M., Quidelleur, X., Khadri, S.F.R., Subbarao, K.V. and Thordarson, T., 2009. Determination of rapid Deccan eruptions across the KTB using paleomagnetic secular variation:(II) Constraints from analysis of 8 new sections and synthesis for a 3500m-thick composite section. Journal of Geophysical Research: Solid Earth, 114(B6), p.B06103.

Chenet, A.L., Quidelleur, X., Fluteau, F., Courtillot, V. and Bajpai, S., 2007. 40K–40Ar dating of the Main Deccan large igneous province: Further evidence of KTB age and short duration. Earth and Planetary Science Letters, 263(1-2), pp.1-15.

Closs, H., Bungenstock, H. and Hinz, K., 1969. Ergebnisse seismischer Untersuchungen im nördlichen Arabischen Meer, ein Beitrag zur Internationalen Indischen Ozean Expedition. Meteor Forschungsergebnisse: Reihe C, Geologie und Geophysik, 2, pp.1-28. A: Mathematical, Physical and Engineering Sciences, 374(2081), p.20160035.

Colleps, C. L., McKenzie, N. R., Guenthner, W. R., Sharma, M., Gibson, T. M., & Stockli, D. F. (2021). Apatite (U-Th)/He thermochronometric constraints on the northern extent of the Deccan large igneous province. Earth and Planetary Science Letters, 571, 117087. https://doi.org/10.1016/j.epsl.2021.117087

Courtillot, V., Besse, J., Vandamme, D., Montigny, R., Jaeger, J.J. and Cappetta, H., 1986. Deccan flood basalts at the Cretaceous/Tertiary boundary?. Earth and Planetary Science Letters, 80(3-4), pp.361-374.

Courtillot, V., 1990. Deccan volcanism at the Cretaceous-Tertiary boundary: past climatic crises as a key to the future? Palaeogeography, Palaeoclimatology, Palaeoecology, 89(3), pp.291-299.

Cox, K.G. and Hawkesworth, C.J., 1985. Geochemical stratigraphy of the Deccan Traps at Mahabaleshwar, Western Ghats, India, with implications for open system magmatic processes. *Journal of Petrology*, *26*(2), pp.355-377.

Crawford, A.R., 1971. Gondwanaland and the growth of India. Geological Society of India, 12(3), pp.205-221.

Damer, B. and Deamer, D., 2020. The hot spring hypothesis for an origin of life. Astrobiology, 20(4), pp.429-452.

Das, P., Maya, K. and Padmalal, D., 2021. Hydrochemistry, geothermometry and origin of the low temperature thermal springs of South Konkan region, India. Geothermics, 90, p.101997.

Das, A., Krishnaswami, S., Sarin, M.M. and Pande, K., 2005. Chemical weathering in the Krishna Basin and Western Ghats of the Deccan Traps, India: Rates of basalt weathering and their controls. Geochimica et Cosmochimica Acta, 69(8), pp.2067-2084.

Das, S.R. and Ray, A.K., 1977. Fracture pattern within Deccan Trap and West Coast of India. Geological Survey of India Miscellaneous Publication, 31, pp.77-79.

Das, S.R. and RAY, A.K., 1973. Photogeological interpretation of structure and tectonics of the Koyna region and part of west coast, Maharashtra. India. Rec. Geol. Surv. India, 105, pp.83-94.

Dessai, A.G. and Bertrand, H., 1995. The “Panvel Flexure” along the Western Indian continental margin: an extensional fault structure related to Deccan magmatism. Tectonophysics, 241(1-2), pp.165-178.

Dessert, C., Dupré, B., Gaillardet, J., François, L.M. and Allègre, C.J., 2003. Basalt weathering laws and the impact of basalt weathering on the global carbon cycle. Chemical Geology, 202(3-4), pp.257-273.

Dotsika, E., Dalampakis, P., Spyridonos, E., Diamantopoulos, G., Karalis, P., Tassi, M., Raco, B., Arvanitis, A., Kolios, N. and Michelot, J.L., 2021. Chemical and isotopic characterization of the thermal fluids emerging along the North–Northeastern Greece. *Scientific reports*, *11*(1), p.16291.

Du, J., Liu, C., Fu, B., Ninomiya, Y., Zhang, Y., Wang, C., Wang, H. and Sun, Z., 2005. Variations of geothermometry and chemical-isotopic compositions of hot spring fluids in the Rehai geothermal field, southwestern China. Journal of Volcanology and Geothermal Research, 142(3-4), pp.243-261.

Ellis, A.J. and Mahon, W.A.J., 1964. Natural hydrothermal systems and experimental hot-water/rock interactions. Geochimica et Cosmochimica Acta, 28(8), pp.1323-1357.

Ellis, A.J. and Mahon, W.A.J., 1967. Natural hydrothermal systems and experimental hot water/rock interactions (Part II). Geochimica et Cosmochimica Acta, 31(4), pp.519-538.

Evans, M.J., Derry, L.A. and France-Lanord, C., 2004. Geothermal fluxes of alkalinity in the Narayani river system of central Nepal. Geochemistry, Geophysics, Geosystems, 5(8).

Evans, M.J., Derry, L.A., Anderson, S.P. and France-Lanord, C., 2001. Hydrothermal source of radiogenic Sr to Himalayan rivers. Geology, 29(9), pp.803-806.

Evans, M.J., Derry, L.A. and France-Lanord, C., 2008. Degassing of metamorphic carbon dioxide from the Nepal Himalaya. Geochemistry, Geophysics, Geosystems, 9(4).

Ferrier, K.L., Kirchner, J.W. and Finkel, R.C., 2012. Weak influences of climate and mineral supply rates on chemical erosion rates: Measurements along two altitudinal transects in the Idaho Batholith. Journal of Geophysical Research: Earth Surface, 117(F2).

Fournier, R.O., 1966. Estimation of underground temperatures from the silica content of water from hot springs and wet-steam wells. Amer. J. Sci., 264, pp.685-697.

Fournier, R.O. and Marshall, W.L., 1983. Calculation of amorphous silica solubilities at 25 to 300 C and apparent cation hydration numbers in aqueous salt solutions using the concept of effective density of water. Geochimica et Cosmochimica Acta, 47(3), pp.587-596.

France-Lanord, C., Evans, M., Hurtrez, J.E. and Riotte, J., 2003. Annual dissolved fluxes from Central Nepal rivers: budget of chemical erosion in the Himalayas. Comptes rendus. Géoscience, 335(16), pp.1131-1140.

Frings, P.J. and Buss, H.L., 2019. The central role of weathering in the geosciences. *Elements: An International Magazine of Mineralogy, Geochemistry, and Petrology*, *15*(4), pp.229-234.

Gaillardet, J., Dupré, B., Louvat, P. and Allegre, C.J., 1999. Global silicate weathering and CO2 consumption rates deduced from the chemistry of large rivers. Chemical geology, 159(1-4), pp.3-30.

Gaillardet, J. and Galy, A., 2008. Himalaya--Carbon Sink or Source?. *Science*, *320*(5884), pp.1727-1728.

Galy, A. and France-Lanord, C., 1999. Weathering processes in the Ganges–Brahmaputra basin and the riverine alkalinity budget. Chemical Geology, 159(1-4), pp.31-60.

German, C.R., Casciotti, K.A., Dutay, J.C., Heimbürger, L.E., Jenkins, W.J., Measures, C.I., Mills, R.A., Obata, H., Schlitzer, R., Tagliabue, A. and Turner, D.R., 2016. Hydrothermal impacts on trace element and isotope ocean biogeochemistry. Philosophical Transactions of the Royal Society

Gibbs, R.J., 1970. Mechanisms controlling world water chemistry. Science, 170(3962), pp.1088-1090.

Gislason, S.R., Arnórsson, S. and Ármannsson, H., 1996. Chemical weathering of basalt in Southwest Iceland; effects of runoff, age of rocks and vegetative/glacial cover. American Journal of Science, 296(8), pp.837-907.

Gorman, P.J., Kerrick, D.M. and Connolly, J.A.D., 2006. Modeling open system metamorphic decarbonation of subducting slabs. *Geochemistry, Geophysics, Geosystems*, *7*(4).

Grossman, R.L. and Durran, D.R., 1984. Interaction of low-level flow with the western Ghat Mountains and offshore convection in the summer monsoon. Monthly Weather Review, 112(4), pp.652-672.

Gupta, M.L. and Sukhija, B.S., 1974. Preliminary studies of some geothermal areas in India. Geothermics, 3(3), pp.105-112.

Gupta, H.K. and Roy, S., 2006. Geothermal energy: an alternative resource for the 21st century. Elsevier.

Gurav, T., Singh, H.K. and Chandrasekharam, D., 2016. Major and trace element concentrations in the geothermal springs along the west coast of Maharashtra, India. Arabian Journal of Geosciences, 9, pp.1-15.

Han, Y., Wang, G., Cravotta III, C.A., Hu, W., Bian, Y., Zhang, Z. and Liu, Y., 2013. Hydrogeochemical evolution of Ordovician limestone groundwater in Yanzhou, North China. Hydrological Processes, 27(16), pp.2247-2257.

Hartmann, J. and Moosdorf, N., 2012. The new global lithological map database GLiM: A representation of rock properties at the Earth surface. Geochemistry, Geophysics, Geosystems, 13(12).

Hren, M.T., Chamberlain, C.P., Hilley, G.E., Blisniuk, P.M. and Bookhagen, B., 2007. Major ion chemistry of the Yarlung Tsangpo–Brahmaputra River: chemical weathering, erosion, and CO2 consumption in the southern Tibetan plateau and eastern syntaxis of the Himalaya. *Geochimica et Cosmochimica Acta*, *71*(12), pp.2907-2935.

Irwin, W.P. and Barnes, I., 1980. Tectonic relations of carbon dioxide discharges and earthquakes. Journal of Geophysical Research: Solid Earth, 85(B6), pp.3115-3121.

Jay, A.E. and Widdowson, M., 2008. Stratigraphy, structure and volcanology of the SE Deccan continental flood basalt province: implications for eruptive extent and volumes. Journal of the Geological Society, 165(1), pp.177-188.

Keller, G., Adatte, T., Bajpai, S., Mohabey, D.M., Widdowson, M., Khosla, A., Sharma, R., Khosla, S.C., Gertsch, B., Fleitmann, D. and Sahni, A., 2009. K–T transition in Deccan Traps of central India marks major marine Seaway across India. Earth and Planetary Science Letters, 282(1-4), pp.10-23.

Khosla, A. and Sahni, A., 2003. Biodiversity during the Deccan volcanic eruptive episode. Journal of Asian Earth Sciences, 21(8), pp.895-908.

Krishnaswami, S., 1999. Silicate weathering in the Himalaya: Role in contributing to major ions and radiogenic Sr to the Bay of Bengal. Ocean science, trends and future directions.

Kale, V.S., Chatterjee, P. and Pande, K., 2020. Emplacement history and evolution of the Deccan Volcanic Province, India. Episodes Journal of International Geoscience, 43(1), pp.278-299.

Laidler, K.J., Chemical Kinetics (Harper & Row 1987) (pp. 507-8). ISBN 0-06-043862-2.

Li, C., Kang, S., Chen, P. et al. Geothermal spring causes arsenic contamination in river waters of the southern Tibetan Plateau, China. Environ Earth Sci 71, 4143–4148 (2014). https://doi.org/10.1007/s12665-013-2804-2

Louvat, P. and Allègre, C.J., 1997. Present denudation rates on the island of Reunion determined by river geochemistry: basalt weathering and mass budget between chemical and mechanical erosions. Geochimica et Cosmochimica Acta, 61(17), pp.3645-3669.

Louvat, P. and Allègre, C.J., 1998. Riverine erosion rates on Sao Miguel volcanic island, Azores archipelago. Chemical Geology, 148(3-4), pp.177-200.

Low, U., Absar, A., Duraiswami, R. and Singh, A., 2020. Geophysical exploration of Tural-Rajwadi group of hot springs, West Coast Geothermal Province, Maharashtra, India and its implications. *Geothermics*, *88*, p.101874.

Lü, Y., Zheng, M., Zhao, P. and Xu, R., 2014. Geochemical processes and origin of boron isotopes in geothermal water in the Yunnan-Tibet geothermal zone. *Science China Earth Sciences*, *57*, pp.2934-2944.

Mahon, W.A.J., 1966. Silica in hot water discharged from drillholes at Wairakei, New Zealand. New Zealand Jour. Sci, 9, pp.135-144.

Mahoney, J.J., 1988. Deccan Traps. In: J.D. MacDougall (Editor), Continental Flood Basalts. Kluwer, Dordrecht, pp. 151~194.

Majumdar, N., Mukherjee, A.L. and Majumdar, R.K., 2009. Mixing hydrology and chemical equilibria in Bakreswar geothermal area, Eastern India. Journal of Volcanology and geothermal Research, 183(3-4), pp.201-212.

Martinelli, G. and Dadomo, A., 2017. Factors constraining the geographic distribution of earthquake geochemical and fluid-related precursors. Chemical Geology, 469, pp.176-184.

Marty, B. and Tolstikhin, I.N., 1998. CO2 fluxes from mid-ocean ridges, arcs and plumes. *Chemical Geology*, *145*(3-4), pp.233-248.

Millot, R., Érôme Gaillardet, J., Dupré, B. and Allègre, C.J., 2003. Northern latitude chemical weathering rates: clues from the Mackenzie River Basin, Canada. Geochimica et Cosmochimica Acta, 67(7), pp.1305-1329.

Millero, F.J., 1974. The physical chemistry of seawater. Annual Review of Earth and Planetary Sciences, 2(1), pp.101-150.

Minissale, A., Vaselli, O., Chandrasekharam, D., Magro, G., Tassi, F. and Casiglia, A., 2000. Origin and evolution of 'intracratonic'thermal fluids from central-western peninsular India. Earth and Planetary Science Letters, 181(3), pp.377-394.

Mitchell, C. and Widdowson, M., 1991. A geological map of the southern Deccan Traps, India and its structural implications. *Journal of the Geological Society*, *148*(3), pp.495-505.

Muthuraman, K., 1986. Sea water—Basalt interactions and genesis of the coastal thermal waters of Maharashtra, India. Geothermics, 15(5-6), pp.689-703.

Monterio, A.J., Duraiswami, R.A., Pujari, S.J., Absar, A., Low, U. and Karmalkar, N.R., 2019, March. Petrophysical variations within the basaltic lava flows from Tural-Rajawadi hot springs, Western India and their bearing on the viability of low-enthalpy geothermal systems. In *IOP Conference Series: Earth and Environmental Science* (Vol. 249, No. 1, p. 012004). IOP Publishing.

Morey, G.W., Fournier, R.O. and Rowe, J.J., 1962. The solubility of quartz in water in the temperature interval from 25 to 300 C. Geochimica et Cosmochimica Acta, 26(10), pp.1029-1043.

Naik, P.K., Awasthi, A.K. and Mohan, P.C., 2002. Springs in a headwater basin in the Deccan Trap country of the Western Ghats, India. Hydrogeology Journal, 10, pp.553-565.

Négrel, P., Allègre, C.J., Dupré, B. and Lewin, E., 1993. Erosion sources determined by inversion of major and trace element ratios and strontium isotopic ratios in river water: the Congo Basin case. Earth and Planetary Science Letters, 120(1-2), pp.59-76.

Newell, D.L., Jessup, M.J., Cottle, J.M., Hilton, D.R., Sharp, Z.D. and Fischer, T.P., 2008. Aqueous and isotope geochemistry of mineral springs along the southern margin of the Tibetan plateau: implications for fluid sources and regional degassing of CO2. Geochemistry, Geophysics, Geosystems, 9(8).

Nicholson, K., 2012. Geothermal fluids: chemistry and exploration techniques. Springer Science & Business Media.

Oliva, P., Viers, J. and Dupré, B., 2003. Chemical weathering in granitic environments. Chemical geology, 202(3-4), pp.225-256.

Pande, K., Yatheesh, V. and Sheth, H., 2017. 40Ar/39Ar dating of the Mumbai tholeiites and Panvel flexure: intense 62.5 Ma onshore–offshore Deccan magmatism during India-Laxmi Ridge–Seychelles breakup. Geophysical Journal International, 210(2), pp.1160-1170.

Piper, A.M., 1944. A graphic procedure in the geochemical interpretation of water-analyses. Eos, Transactions American Geophysical Union, 25(6), pp.914-928.

Quade, J., English, N. and DeCelles, P.G., 2003. Silicate versus carbonate weathering in the Himalaya: a comparison of the Arun and Seti River watersheds. Chemical Geology, 202(3-4), pp.275-296.

Raymo, M.E. and Ruddiman, W.F., 1992. Tectonic forcing of late Cenozoic climate. nature, 359(6391), pp.117-122.

Reddy, D.V., Nagabhushanam, P. and Ramesh, G., 2013. Turnover time of Tural and Rajvadi hot spring waters, Maharashtra, India. Current Science, pp.1419-1424.

Reddy, S.K.K., Gupta, H. and Reddy, D.V., 2019. Dissolved inorganic carbon export by mountainous tropical rivers of the Western Ghats, India. Chemical Geology, 530, p.119316.

Roy, S. and Rao, R.U.M., 2000. Heat flow in the Indian shield. Journal of Geophysical Research: Solid Earth, 105(B11), pp.25587-25604.

Ruggero Bertani,World geothermal power generation in the period 2001–2005,Geothermics,Volume 34, Issue 6,2005,Pages 651-690,ISSN 0375-6505,https://doi.org/10.1016/j.geothermics.2005.09.005.

Shah, M., Sircar, A., Shaikh, N., Patel, K., Sharma, D. and Vaidya, D., 2019. Comprehensive geochemical/hydrochemical and geo-thermometry analysis of Unai geothermal field, Gujarat, India. Acta Geochimica, 38, pp.145-158.

Saha, G., Kumar, V., Chaubey, D. K., & Rai, S. S. (2023). Cryptic magma chamber in the Deccan Traps imaged using receiver functions and surface wave dispersion. Geophysical Research Letters, 50, e2023GL105359. https://doi. org/10.1029/2023GL105359

Sarker, R.P., 1966. A dynamical model of orographic rainfall. Monthly weather review, 94(9), pp.555-572.

Schopka, H.H., Derry, L.A. and Arcilla, C.A., 2011. Chemical weathering, river geochemistry and atmospheric carbon fluxes from volcanic and ultramafic regions on Luzon Island, the Philippines. Geochimica et Cosmochimica Acta, 75(4), pp.978-1002.

Sen, G., 2001. Generation of Deccan trap magmas. Journal of Earth System Science, 110, pp.409-431.

Singh, H.K., Kumar, Y., Chandrasekharam, D., Gurav, T. and Singh, B., 2014. High-heat-producing granites of East Dharwar Craton around Gugi, Karnataka, and their possible influence on the evolution of Rajapur thermal springs, Deccan Volcanic Province, India. *Geothermal Energy*, *2*, pp.1-12.

Subbarao, K.V. and Courtillot, V., 2017. Deccan basalts in and around Koyna—Warna region, Maharashtra: Some reflections. Journal of the Geological Society of India, 90(6), pp.653-662.

Tawde, S.A. and Singh, C., 2015. Investigation of orographic features influencing spatial distribution of rainfall over the Western Ghats of India using satellite data. International Journal of Climatology, 35(9), pp.2280-2293.

Tipper, E.T., Bickle, M.J., Galy, A., West, A.J., Pomiès, C. and Chapman, H.J., 2006. The short term climatic sensitivity of carbonate and silicate weathering fluxes: insight from seasonal variations in river chemistry. Geochimica et Cosmochimica Acta, 70(11), pp.2737-2754.

Tiwari, S.K., Rai, S.K., Bartarya, S.K., Gupta, A.K. and Negi, M., 2016. Stable isotopes (δ13CDIC, δD, δ18O) and geochemical characteristics of geothermal springs of Ladakh and Himachal (India): Evidence for CO2 discharge in northwest Himalaya. Geothermics, 64, pp.314-330.

Tamburello, G., Chiodini, G., Ciotoli, G., Procesi, M., Rouwet, D., Sandri, L., Carbonara, N. and Masciantonio, C., 2022. Global thermal spring distribution and relationship to endogenous and exogenous factors. Nature Communications, 13(1), p.6378.

Wei, Z., Huang, S., Xu, J., Yuan, C., Zhang, M. and Wang, C., 2024. Geochemical evolution of geothermal waters in the Pearl River Delta region, South China: Insights from water chemistry and isotope geochemistry. *Journal of Hydrology: Regional Studies*, *51*, p.101670.

White, R. and McKenzie, D., 1989. Magmatism at rift zones: the generation of volcanic continental margins and flood basalts. Journal of Geophysical Research: Solid Earth, 94(B6), pp.7685-7729.

White, A.F. and Blum, A.E., 1995. Effects of climate on chemical_ weathering in watersheds. Geochimica et cosmochimica acta, 59(9), pp.1729-1

8 Annexure

Table3: Major Ions,silica concentration data for hot spring water,river water, and groundwater samples of deccan region ,Maharashtra,India

					Na	K	Ca	Mg	F^-	Cl^-	NO_3^{2-}	SO_4^{2-}	HCO_3^-	SiO_2	TDS	TZ+	TZ-	TZ+/TZ-	NICB
Type	**Sample Id**	**pH**	**T(˚C)**	**Elevation(m)**	μM										mg/L	μEq			%
Hotspring																			
	HS23/01	7.25	41.1	12	3410	365	579	308	51	400	16	47	4640	413	427	5549	5201	1.1	6
	HS23/02	7.86	34.3	16	12423	232	1509	13	311	14124	14	280	915	888	946	15701	15923	1.0	-1
	HS23/03	7.9	49.1	37	10160	224	1223	bdl	159	10378	bdl	1137	705	1521	815	12830	13516	0.9	-5
	HS23/04	7.63	55.4	31	7211	132	1250	51	167	9370	bdl	1120	804	1495	714	9946	12581	0.8	-23
	HS23/05	8.92	42.9	21	6876	122	221	bdl	198	4925	106	886	738	1285	487	7440	7739	1.0	-4
	HS23/06	8.86	46.3	17	6693	107	304	bdl	198	4893	bdl	910	702	1209	478	7408	7614	1.0	-3
	HS23/07	7.76	60	23	24390	483	4684	27	91	29171	365	1473	257	1052	1984	34293	32830	1.0	4
	HS23/08	7.54	40.01	20	21433	299	8979	58	167	34513	282	1554	487	982	2289	39806	38557	1.0	3
	HS23/09	7.66	43.2	18	46516	369	45792	116	76	141263	448	1878	184	812	8151	138700	145728	1.0	-5
	HS23/10	8.78	38.3	8	19495	214	4505	4	102	24148	bdl	1473	229	845	1651	28727	27425	1.0	5
	HS23/11	8.5	49	21	19495	236	4087	bdl	129	23590	bdl	1352	242	981	1605	27905	26665	1.0	5
	HS23/12	8.45	46	16	15723	215	4027	8	167	19684	697	1392	279	1053	1426	24008	23612	1.0	2
River																			
	RBHS23/01	6.76	32.4	5	176	bdl	215	145	4	110	7	19	709	364	66	897	868	1.0	3
	RBHS23/02	7.4	29.9	14	186	24	190	152	4	107	16	18	827	418	74	895	989	0.9	10
	RBHS23/04	7.19	32.1	31	520	22	268	176	12	434	24	56	956	568	109	1431	1538	0.9	7
	RBHS23/05	6.63	31.1	24	153	10	197	135	6	86	14	20	742	396	66	828	888	0.9	7
	RBHS23/08	8.22	30.8	1	402	17	552	501	12	175	7	53	2368	703	201	2525	2668	0.9	6
	RBHS23/09	8.11	32.6	18	514	11	622	447	12	324	bdl	59	2373	728	210	2664	2826	0.9	6
	RBHS23/10	7.84	33.5	12	382	11	520	439	10	178	12	38	2198	687	186	2310	2474	0.9	7
	RBHS23/11	7.22	29.9	18	274	18	332	230	8	155	13	25	1284	494	113	1416	1510	0.9	6
	RAHS23/01	7.4	32	3	176	bdl	171	148	3	110	12	19	713	359	65	814	875	0.9	7
	RAHS23/02	6.61	29.4	1	272	11	202	154	8	182	12	34	796	423	78	995	1065	0.9	7
	RAHS23/03	6.61	30.1	41	394	11	227	151	10	304	19	41	861	442	91	1162	1276	0.9	9
	RAHS23/04	7.48	47	31	6444	136	806	82	120	6360	40	723	860	1187	540	8356	8826	0.9	5
	RAHS23/05	7.45	31.1	15	160	13	178	141	bdl	89	19	17	753	394	67	811	895	0.9	10
	RAHS23/09	8.26	32.5	19	555	13	684	451	12	499	6	59	2361	725	220	2839	2996	0.9	5

	RAHS23/10	8.21	31.5	2	23093	515	992	2938	12	31069	17	1372	1893	564	2012	31469	35737	0.9	13
	RAHS23/11	8.36	30.9	18	431	19	369	232	8	360	9	38	1327	499	129	1652	1780	0.9	7
Groundwater																			
	HSGW23/01	6.56	33.4	14	1518	bdl	192	115	24	416	13	91	1547	622	164	2131	2181	1.0	2
	HSGW23/02	6.99	31.5	22	663	27	1137	577	10	456	145	80	3650	752	332	4117	4421	0.9	7

Table 4: Comparison between measured data with Himalayan, other peninsular and Global data

Hotspring Sample No. #	Type	Temp (°C)	pH	Cond (µS/cm)	µM Na	K	Ca	Mg	F	Cl	NO_3	SO_4	HCO_3^-	SiO_2	TDS(mg/L)	Source
Deccan Measured	**Min**				3410	132	221	116	51	400	14	47	184	413	427	
	Max				46516	365	45792	308	311	141263	697	1878	4640	1521	8137	
	Avg	45	8		16152	240	6430	212	151	26372	275	1125	848	1045	1740	
	Std Dev	7	1		11708	118	12658	136	69	37685	252	531	1222	307	2107	
Deccan Previously Reported	**Avg**	52	8		18132	245	8000	93	127	32049		1399	694	1092	2085	Gurav et al.,2015
Himalayan HS	**Avg**	49	7	1795	18660	1963	3653	778	189	19643	48	1461	7390	2124	1876	Becker et al.,2007;Tiwari et al.,2016
	Std Dev	19	1	1825	22979	3087	5553	1130	227	29239	88	2627	8614	1017	2072	
Other Peninsular	**Avg**	53	8	871	9515	207	1415	112	331	9470		735	934	1851	775	Minissale et al.2000;Singh et al.2020;Zimick et al.2017;Shah et al.2019;Majumdar et al.2015
	Std Dev	15	1	632	11496	257	2817	219	300	15820		820	698	446	1155	
Global HS	**Avg**	52	6		63553	3317	7199	7021		78246	8924	10575	10694	2921	5304	Tamburello et at.2022; Nicholson;Kaasalainen & Stefánsson 2012;J.Du et al.2004
	Std Dev	26	3		176904	9325	15644	29945		249440	19295	55604	5201	2800	12003	
Deccan Expected /Measured		1.1	1.0		1	1	1	0	1	1		1	1	1	1	
Himalayan/Measured or Vice Versa		1.1	0.9		1	8	2	4	1	1	6	1	9	2	1	
Peninsular/Measured or Vice Versa		1.2	1.0		2	1	5	2	2	3		2	1	2	2	

Global/Measured or Vice Versa		1.2	0.7		4	14	1	33		3	32	9	13	3	3	

River

					μM											
Sample No. #	**Type**	**Temp (°C)**	**pH**	**Cond (μS/cm)**	**Na**	**K**	**Ca**	**Mg**	**F**	**Cl**	**NO_3**	**SO_4**	**HCO_3^-**	**SiO_2**	**TDS(mg/L)**	
Measured	**Min**	29	7		153	10	171	82	3	86	6	17	709	359	65	
	Max	47	8		23093	515	992	2938	120	31069	40	1372	2373	1187	2012	
	Avg	32	7		2133	59	408	408	16	2534	15	162	1314	559	264	
	Std Dev	4	1		5795	135	258	689	29	7763	9	366	676	213	481	
Global Averaged	**Avg**				244	36	351	143		144		102	908	127		Tripathy and Das .,2014
Measured /Global or vice versa					9	2	1	3		18		2	1	4		

Table5: Calculated solute flux from the major ion data

Type	Sample Id	Location	Solute Concentration(µM)						Discharge (m^3/a)	moles/yr					
			Na	Ca	Cl^-	SO_4^{2-}	HCO_3^-	TDS		Na	Ca	Cl	SO_4	HCO_3	TDS
	Hot spring water														
1	HS23/01	Rajapur-Unhale	3.41	0.58	0.40	0.05	4.64	10							
2	HS23/02	Anjhaneri Math	12.42	1.51	14.12	0.28	0.91	30							
3	HS23/03	Rajwadi	10.16	1.22	10.38	1.14	0.71	24	1.40E+05	1.43E+06	1.72E+05	1.46E+06	1.59E+05	9.90E+04	3.37E+06
4	HS23/04	Tural	7.21	1.25	9.37	1.12	0.80	20	1.96E+05	1.41E+06	2.44E+05	1.83E+06	2.19E+05	1.57E+05	3.93E+06
5	HS23/05	Aravalli	6.88	0.22	4.93	0.89	0.74	14	3.78E+04	2.60E+05	8.35E+03	1.86E+05	3.35E+04	2.79E+04	5.33E+05
6	HS23/06	Kokare	6.69	0.30	4.89	0.91	0.70	14							
7	HS23/07	Unhavre-Farare	24.39	4.68	29.17	1.47	0.26	61	4.57E+05	1.12E+07	2.14E+06	1.33E+07	6.74E+05	1.17E+05	2.79E+07
8	HS23/08	Akloli-Vajreswari	21.43	8.98	34.51	1.55	0.49	68							
9	HS23/09	Koknere	46.52	45.79	141.26	1.88	0.18	237							
10	HS23/10	Padusapada	19.50	4.50	24.15	1.47	0.23	50							
11	HS23/11	Sativili	19.50	4.09	23.59	1.35	0.24	49							
12	HS23/12	Ganespuri	15.72	4.03	19.68	1.39	0.28	42	2.05E+05	3.22E+06	8.26E+05	4.03E+06	2.85E+05	5.72E+04	8.65E+06
	River Water														
13	RBHS23/01	Arjuna River	0.18	0.22	0.11	0.02	0.71	1	1.90E+09	3.34E+08	4.09E+08	2.09E+08	3.60E+07	1.35E+09	2.63E+09
14	RBHS23/02	Kajali river	0.19	0.19	0.11	0.02	0.83	2	1.68E+09	3.12E+08	3.20E+08	1.79E+08	3.05E+07	1.39E+09	2.56E+09
15	RBHS23/04	Canal joining creek which finally end up in Bav River	0.52	0.27	0.43	0.06	0.96	2							
16	RBHS23/05	Jaigad river	0.15	0.20	0.09	0.02	0.74	1							

17	RBHS23/08	Tansa river	0.40	0.55	0.18	0.05	2.37	4							
18	RBHS23/09	Surya river	0.51	0.62	0.32	0.06	2.37	4							
19	RBHS23/10	Vaitarna river	0.38	0.52	0.18	0.04	2.20	4	4.37E+09	1.67E+09	2.27E+09	7.80E+08	1.64E+08	9.61E+09	1.66E+10
20	RBHS23/11	Creek Joining Vaitarna	0.27	0.33	0.15	0.03	1.28	2	4.37E+09	1.20E+09	1.45E+09	6.75E+08	1.11E+08	5.61E+09	1.02E+10
21	RAHS23/01	Arjuna River	0.18	0.17	0.11	0.02	0.71	1	1.90E+09	3.34E+08	3.25E+08	2.09E+08	3.60E+07	1.35E+09	2.57E+09
22	RAHS23/02	Kajali river	0.27	0.20	0.18	0.03	0.80	2	1.68E+09	4.56E+08	3.40E+08	3.05E+08	5.63E+07	1.34E+09	2.81E+09
23	RAHS23/03	Creek joining Bav river	0.39	0.23	0.30	0.04	0.86	2							
24	RAHS23/04	canal joining creek which finally end up in Bav River	6.44	0.81	6.36	0.72	0.86	16							
25	RAHS23/05	Jaigad river	0.16	0.18	0.09	0.02	0.75	1							
26	RAHS23/09	Surya river	0.56	0.68	0.50	0.06	2.36	5							
28	RAHS23/11	Vaitarna river	0.43	0.37	0.36	0.04	1.33	3	4.37E+09	1.88E+09	1.61E+09	1.57E+09	1.64E+08	5.80E+09	1.22E+10
	HS Average									3.49E+06	6.78E+05	4.17E+06	2.74E+05	9.17E+04	8.87E+06
	River Average									8.83E+08	9.62E+08	5.62E+08	8.54E+07	3.78E+09	7.08E+09
	River/HS Average									2.53E+02	1.42E+03	1.35E+02	3.12E+02	4.12E+04	7.98E+02

Table6: Average accuracy and precission for the analysis

Parameters	Accuracy (%)	Precission(%)	Error (%)	Precission(%)
Na	1	1	1	1
	3	0	3	0
	0		0	
	2		2	
Average	1	1		
K	1	9	1	9
	1		1	
	1		1	
Average	1			
Ca	10	2	10	2
	8		8	
	10		10	
Average	9	2		
Mg	1	1	1	1
	2	8	2	8
	0		0	
	1		1	
Average	1	5		
F	0	0	0	0
	0		0	
	0		0	
	0		0	
Average	0	0		
Cl	2	6	2	6
	1		1	

	0		0	
	1		1	
	1		1	
Average	1	6		
NO_3	4	0	4	0
	4	0	4	0
	4		4	
	4		4	
Average	4	0		
SO_4	4	1	4	1
	1		1	
	6		6	
	1		1	
Average	3	1		
HCO_3	0	0	0	0
	0	3	0	3
	0	0	0	0
	1	0	1	0
	2		2	
	1		1	
Average	0	1		
SiO_2	2	0	2	0
	2	1	2	1
	5		5	
	3		3	
	5		5	
Average	4	1		
Overall Average			*2*	*2*

Table7: Calculation of reservoir temperature.

			NoSteam Loss	Max steam Loss	Truesdell (1976)	Tonani (1980)	Arnorsson (1983)	Fournier (1979b)	Nieva & Nieva (1987)	Giggenbach (1988)
Type	**Sample Id**	**Location**	**SiO_2**	**SiO_2**	**Na/K**	**Na/K**	**Na/K**	**Na/K**	**Na/K**	**Na/K**
1	HS23/01	Rajapur-Unhale	72	76	263	308	275	275	260	285
2	HS23/02	Anjhaneri Math	105	105	90	115	143	135	124	155
3	HS23/03	Rajwadi	132	129	102	127	153	145	134	165
4	HS23/04	Tural	134	130	89	113	142	134	123	154
5	HS23/05	Aravalli	123	121	87	111	141	132	121	152
6	HS23/06	Kokare	120	118	80	103	135	126	115	146
7	HS23/07	Unhavre-Farare	113	112	94	119	147	139	127	158
8	HS23/08	Akloli-Vajreswari	110	109	72	94	127	119	108	139
9	HS23/09	Koknere	101	102	41	60	100	90	80	111
10	HS23/10	Padusapada	103	103	58	79	115	106	95	127
11	HS23/11	Sativili	110	109	64	85	120	111	100	131
12	HS23/12	Ganespuri	113	112	71	93	126	118	107	138
	Average		111	111	93	117	144	136	124	155
	Average			111				128		

Table 08: CO_2 flux of Deccan hot spring and comparison with NW Himalayan hot springs

Sl No	Sample Id	Location	DIC(mM/Kg)	Discharge (L/S)	Discharge (m^3/a)	Direct DIC Flux(mole/a)	CO_2 Flux(mole/a)	CO_2 Flux(mole/a/km^2)	Area(km^2)	Source
3	HS23/03	Rajwadi	0.7	4.5	1.403E+05	9.900E+04	9.900E+04			Low et al.,2020
4	HS23/04	Tural	0.8	6.2	1.955E+05	1.572E+05	1.572E+05		1.5	
5	HS23/05	Aravalli	0.7	1.2	3.784E+04	2.792E+04	2.792E+04			
7	HS23/07	Unhavre-Farare	0.3	14.5	4.573E+05	1.173E+05	1.173E+05			
11	HS23/11	Sativili	0.2	7	2.050E+05	4.968E+04	4.968E+04			
	Sum					4.511E+05	4.511E+05			
	Tural Rajwadi Release rate						2.562E+05	1.708E+05		
	CO_2 Consumption Rate							360000		Das et al.,2005
	Consumption /Release							2		

Sl No	Sample Id	Location	C_{excess}(moles/L)	Discharge (L/S)	Discharge (L/a)	CO_2 Flux(mole/a)
3	HS23/03	Rajwadi	0.0006	4.45	1.40E+08	8.69E+04
4	HS23/04	Tural	0.0006	6.2	1.96E+08	1.22E+05
5	HS23/05	Aravalli	0.0014	1.2	3.78E+07	5.31E+04
	Sum					2.62E+05

Geothermal Field	CO_2 Flux(mole/a)	Source

Overall CO_2 Flux(mole/a) combining all the geothermal fields of northwest Himalaya	2.00E+10	(Tiwari et al.,2016)
Overall CO_2 Flux(mole/a) combining all the geothermal fields of Deccan	4.511E+05	(Present Study)
NW Himalayan CO_2 flux/Deccan CO_2 Flux	4.433E+04	

Table 09 : Molar ratio of major ions used in this study.

Type	Sample Id	Location	Ca/HCO_3	$Ca+Mg/HCO_3$	Na/Cl
1	HS23/01	Rajapur-Unhale	0.12	0.19	8.52
2	HS23/02	Anjhaneri Math	1.65	1.66	0.88
3	HS23/03	Rajwadi	1.73	1.73	0.98
4	HS23/04	Tural	1.55	1.62	0.77
5	HS23/05	Aravalli	0.30	0.30	1.40
6	HS23/06	Kokare	0.43	0.43	1.37
7	HS23/07	Unhavre-Farare	18.25	18.36	0.84
8	HS23/08	Akloli-Vajreswari	18.45	18.57	0.62
9	HS23/09	Koknere	248.26	248.89	0.33
10	HS23/10	Padusapada	19.71	19.72	0.81
11	HS23/11	Sativili	16.86		0.83
12	HS23/12	Ganespuri	14.42	14.45	0.80
13	RBHS23/01	Arjuna River	0.30	0.51	0.60

14	RBHS23/02	Kajali river	0.23	0.41	0.74
15	RBHS23/04	Canal joining creek which finally end up in Bav River	0.28	0.46	0.20
16	RBHS23/05	Jaigad river	0.27	0.45	0.78
17	RBHS23/08	Tansa river	0.23	0.44	1.29
18	RBHS23/09	Surya river	0.26	0.45	0.59
19	RBHS23/10	Vaitarna river	0.24	0.44	1.14
20	RBHS23/11	Creek Joining Vaitarna	0.26	0.44	0.77
21	RAHS23/01	Arjuna River	0.24	0.45	0.60
22	RAHS23/02	Kajali river	0.25	0.45	0.50
23	RAHS23/03	Creek joining Bav river	0.26	0.44	0.29
24	RAHS23/04	canal joining creek which finally end up in Bav River	0.94	1.03	0.01
25	RAHS23/05	Jaigad river	0.24	0.42	0.80
26	RAHS23/09	Surya river	0.29	0.48	0.11
27	RAHS23/10	Vaitarna river	0.52	2.08	0.74
28	RAHS23/11	Vaitarna river	0.28	0.45	0.20
	Groundwater				
29	HSGW23/01	Kokare	0.12	0.20	2.65
30	HSGW23/02	katale	0.31	0.47	0.45